NASA CONTRACTOR
REPORT

NASA CR-362

NASA CR-362

A SUPERSONIC/HYPERSONIC AERODYNAMIC INVESTIGATION OF THE SATURN IB/APOLLO UPPER STAGE

by David R. Carlson and William P. Walters

NATIONAL AERONAUTICS AND SPACE ADMINISTRATION · WASHINGTON, D. C. · JANUARY 1966

A SUPERSONIC/HYPERSONIC AERODYNAMIC INVESTIGATION

OF THE SATURN IB/APOLLO UPPER STAGE

By David R. Carlson and William P. Walters

Distribution of this report is provided in the interest of information exchange. Responsibility for the contents resides in the author or organization that prepared it.

NATIONAL AERONAUTICS AND SPACE ADMINISTRATION

A SUPERSONIC/HYPERSONIC AERODYNAMIC
INVESTIGATION OF THE SATURN IB/APOLLO UPPER STAGE

By

David R. Carlson
and
William P. Walters

Northrop Space Laboratories
Huntsville, Alabama

ABSTRACT

The static stability and axial force characteristics of an upper stage Saturn IB/Apollo model were investigated in a series of wind tunnel tests at Mach numbers between 1.93 and 8.05. This report presents and analyzes the results of these small-scale studies. Test procedures and models are described, and consideration of boundary layer characteristics and violated modeling rules yields an assessment of the validity of the data.

Four basic models provided evaluation of the basic launch vehicle character-istics, as well as the effects of two modes of mission abort and jettison of the launch escape system. The launch configuration experienced sudden, strong changes in stability derivatives and axial force coefficients near Mach 5. No similar changes were observed on the other configurations. Effects of Reynolds number, Mach number, and boundary layer trips were obtained for each shape. The faired curves are believed to be valid for full-scale flight of the Saturn IB/Apollo upper stage.

TABLE OF CONTENTS

Page

LIST OF ILLUSTRATIONS

LIST OF TABLES

DEFINITION OF SYMBOLS

Symbol   Definition

C_{A_f} Forebody (total minus base) axial force coefficient; [axial force] $/qS$

C_{mg} Pitching moment coefficient referred to Saturn IB station 1086.157
                (S-IVB gimbal station); [pitching moment] $/qSD$

$C_{mg\alpha}$ Rate of change of C_{mg} with angle of attack, generally at $\alpha = 0°$;
                longitudinal stability derivative; $dC_{mg}/d\alpha$ (deg.$^{-1}$)

C_N Normal force coefficient; [normal force] $/qS$

C_{N_α} Rate of change of C_N with angle of attack, generally at $\alpha = 0°$; normal
                force slope; $dC_N/d\alpha$ (deg.$^{-1}$)

CP/D   Center of pressure (in calibers) forward of Saturn IB station 100 (booster
                gimbal station)

D   Saturn IB reference diameter (booster), 6.54 meters full-scale

M   Mach number

P_∞ Free stream static pressure (N/m^2)

q   Free stream dynamic pressure; $\gamma_2 \, P_\infty \, M^2$ (N/m^2)

Re   Free stream Reynolds number per meter; $\rho_\infty \, U/\mu_\infty$ (m^{-1})

Re_D Free stream Reynolds number based on diameter; $\rho_\infty \, UD/\mu_\infty$

S   Reference area based on diameter; $\frac{\pi}{4} \, D^2$ (m^2)

T_∞ Free stream static temperature (degrees Kelvin)

U   Free stream velocity (m/sec)

α Angle of attack (degrees)

DEFINITION OF SYMBOLS (Cont'd)

Symbol	Definition
γ	Ratio of specific heats, 1.40 for perfect air
μ_∞	Free stream absolute viscosity (N-sec/m^2)
ρ_∞	Free stream static density (kg/m^3)

NONSTANDARD ABBREVIATIONS

CM	Command Module, or Apollo Subsystem; C_1 in model nomenclature
LEM	Lunar Excursion Module, enclosed by 8°37' conical flare adapter behind SM
LES	Launch Escape System, consisting of escape rocket and supporting tower; T_1 in model nomenclature
SM	Service Module, containing support and propulsive systems; jettisoned from Apollo between lunar orbit and terrestrial reentry; S_1 in model nomenclature
CSM	Combined Apollo and Service Module subsystems
$A_4^{8°37'}$	Model nomenclature for S-IVB cylinder and LEM adapter flare
t_3	Model nomenclature for boundary layer trip, consisting of 0.025-cm-diameter spheres applied to either escape rocket or Apollo cone, about halfway between the appropriate nose and cone-cylinder junction
S-IVB	Hydrogen/Oxygen-powered second stage of Saturn IB (and third stage of Saturn V LOR)

A SUPERSONIC/HYPERSONIC AERODYNAMIC INVESTIGATION OF THE SATURN IB/APOLLO UPPER STAGE

By David R. Carlson and William P. Walters

Northrop Space Laboratories

SUMMARY

As the Saturn/Apollo launch vehicle accelerates to hypersonic speeds, a point is reached where stability derivatives and axial force coefficients change suddenly and significantly. The center of pressure moves forward about one vehicle diameter, further decreasing the stability. This sudden change in aerodynamic characteristics is associated with the terminal extent of boundary layer separation from the Launch Escape System (LES).

A series of wind tunnel tests were conducted on four upper stage models at Mach numbers between 1.93 and 8.05. Saturn IB trajectory Reynolds numbers were simulated between Mach 4.0 and 6.1. Off-trajectory conditions were run to assess the effect of Reynolds number variation on the vehicle aerodynamic characteristics. Boundary layer trips were used to induce a turbulent boundary layer. The launch configuration, without booster but with LES, was tested most extensively. To find changes caused by LES jettison and mission abort, the high altitude configuration and two aborted configurations were also tested. Data validity was established by consideration of the general behavior of hypersonic boundary layer separation and the degree of violation of strict rules of similarity. The faired curves are believed to predict validly full-scale aerodynamic characteristics.

The launch configuration experienced sudden, strong changes in stability and axial force near Mach 5. No such jumps occurred on the high altitude or abort configurations; their data agreed well with simple Newtonian theory at hypersonic Mach numbers. Jettison of the LES caused very little change in stability below Mach 5, but was a strong stabilizing influence above Mach 5. The axial force coefficient increased at all Mach numbers, and the increase was large above Mach 5. When LES abort occurred, the center of pressure moved aft, and the axial force coefficient increased from one to five times its pre-abort value. Changes which occurred in Service Module (SM) abort were smaller, and remained fairly constant with Mach number.

SECTION I. INTRODUCTION

The Saturn IB/Apollo is a launch vehicle designed to place the Apollo Command and Service Modules (CSM) and Lunar Excursion Module (LEM) into earth orbit for extended astronaut training. It consists of an uprated Saturn I booster mated to the third stage of the Saturn V Lunar Orbital Rendezvous (LOR) vehicle. This third stage of Saturn V (or second stage of Saturn IB) includes the S-IVB propulsion system; the LEM, enclosed by a conical interstage frustum; the Service Module (SM); the Apollo capsule or Command Module (CM); and the Launch Escape System (LES).

To assist optimization of trajectories and vehicle control, a series of wind tunnel tests was planned and executed. A small-scale (0.78 percent) model of the Saturn IB/Apollo upper stage was tested over a Mach number range of 1.93 through 8.05 in the Marshall Space Flight Center (MSFC) 14-inch Trisonic Wind Tunnel and in the Arnold Engineering Development Center von Karman Facility (AEDC vKF) Tunnel "E." Simulation of the Saturn IB/Apollo trajectory Reynolds numbers was attempted, and was closely achieved between Mach 4 and Mach 6. The results of the study also apply to the Saturn V LOR third stage, with certain reservations, since the Saturn V trajectory was not simulated. At Mach numbers where the trajectory dictates presence of the Saturn IB booster, these results give the upper stage contribution to the whole vehicle.

Three earlier study configurations, devoid of design protuberances and differing in length and LEM frustum angle, were tested in the same facilities. Results and qualitative analyses of those tests were published in References 1 and 2. The present report is concerned with summary static stability data derived from basic force data which were published in References 3 and 4.

Three goals guided this test series: first, the establishment of high-speed static aerodynamic characteristics of the Saturn IB/Apollo upper stages; second, the determination of changes to be expected when the LES is jettisoned or abort is completed; and third, the qualitative probing of the flow field about Saturn for application to other multiple cone-cylinder-frustum vehicle shapes. The abort shapes are interesting primarily from the standpoint of definition of initial conditions for reentry trajectories.

Facility limitations forced acceptance of only small Reynolds numbers excursions. As a result, the effects of Reynolds number variation are known to only a limited extent. Diameter-based Reynolds numbers were far below trajectory values below Mach 4 and far above trajectory values above Mach 6. Still, it is believed that the test conditions produced a turbulent boundary layer in the former range and a laminar boundary layer in the latter, both of which would be expected at trajectory conditions. Simulation of the laminar or turbulent state of the boundary layer is of the

2

utmost importance. Thus, the large deviations from trajectory Reynolds number at both ends of the speed range may not be quite as unfortunate as they seem.

SECTION II. MODELS AND TEST TECHNIQUE

A.   MODEL DESCRIPTION

A model of the Saturn IB/Apollo upper stage was designed on a building block format to enable the four test configurations (Fig. 1) to be easily interchanged. The model designations appear at their bases in Figure 1. In this report, they are referred to as, left to right: Launch Configuration (without booster and interstage skirt), High Altitude Configuration, LES-Abort Configuration, and SM-Abort Configuration. Since the models were mounted on stings, no attempt was made to include base details.

The models incorporate all significant design protuberances, including attitude-control motors on the SM, an instrumentation tunnel, ullage rockets, retro-rockets, and fuel line fairings. While the most recent design of the full-scale vehicle specified an 8° 58' semiangle for the LEM adapter flare, the model semiangle was 8° 37'. This difference is negligible.

In the earlier study (Refs. 1 and 2), trips and high Reynolds numbers were used simultaneously to induce transition. Since only the combined tripping efficiency was reported, these two conditions were varied independently in the present tests. The conditions under which trips were required for transition were thus bracketed. The trips chosen for the model were a single row of 0.025-cm spheres spot welded to the surface of both the launch configuration and the high-altitude configuration. They were applied to the leading cone surface about halfway from the apex to the cone-cylinder shoulder. The type, size, spacing, and location of the trips were chosen from unpublished results of a techniques research study performed by C. Dale Andrews of MSFC. In the case of the launch configuration, trips were both used and deleted at high and low Reynolds numbers. For the high-altitude configuration, the trips were used only for conditions where turbulence was desired. No trips were used on the two abort configurations. All linear dimensions given in Figure 1 are in multiples of the vehicle reference diameter, which is slightly less than the S-IVB sylinder diameter. One caliber is 6.54 meters full-scale and 0.0509 meter model-scale. The models were made entirely of stainless steel, and were supported in both tunnels on metric assemblies which combined a sting, force balance, and water jacket. Figure 2 is a photograph of the launch configuration mounted in the AEDC tunnel.

B. FACILITIES

The tests were performed in the MSFC 14-inch Trisonic Wind Tunnel $(1.92 \leq M \leq 4.96)$ and the AEDC vKF Tunnel "E" $(4.97 \leq M \leq 8.05)$. The tunnels and their components are described in References 5 and 6.

Because the nozzles are contoured and account for boundary layer displacement-thickness growth, the test cores were uniform. The models could be placed at angles of attack of 25° without penetrating the viscous boundary of the test core at any condition. Thus, nozzle viscous effects did not influence the tests. Radial flow and axial gradients, which must be taken into account in angle of attack data taken with conical nozzles (Ref. 7), were absent.

Test parameters, base pressures, and force data were corrected for sting and balance deflection, model weight, and interactions among the moment and axial force gages of the three-component force balance. The data were not corrected for airflow misalignment, which was negligible for these tests. The force and moment data were reduced to coefficients which were referred to a body axis system. The axis system originated at vehicle station 1086.2 (S-IVB gimbal station), which is aft of the second stage base station 1186.8. The reference area and reference diameter were those of the S-IB booster (see list of symbols). The static stability and forebody axial force data analyzed here were derived from the base data of References 3 and 4.

C. TEST CONDITIONS

Figure 3 is a plot of Re_D vs M, including a typical Saturn IB/Apollo full-scale trajectory. The symbols show Reynolds numbers actually achieved in the tests. Table I is a listing of Reynolds numbers based on diameter, and equivalent tunnel free-stream Reynolds numbers per meter as functions of Mach number in the two facilities.

Figure 3 shows that the test Reynolds numbers are much less than trajectory values below Mach 4. However, a turbulent boundary layer and minimal separation exist on the LES at the lower Mach numbers, and this is a close and important duplication of flight conditions. At a constant Reynolds number, an increase of Mach number reduces the probability of a turbulent boundary layer. This effect is explained by the reduction in local, equivalent-flat-plate Reynolds number, accompanying an increase in boundary layer thickness as Mach number and shock wave total-pressure loss increase. Shadowgraphs and test data also support the contention that a laminar boundary layer runs along the LES at Mach numbers above 4, while a turbulent layer occurs at the lower Mach numbers. By the same arguments, the high Reynolds numbers and higher total pressures in the AEDC tests were believed to be effective in inducing a turbulent boundary layer up to Mach 7.

4

Initial data were taken at zero angle of attack. Then the model was pitched down to -4° and data were taken in a pitch-pause procedure as the model attitude increased to a maximum angle of 24°. No pitch-pause data were taken at decreasing attitude sweeps; thus hysteresis effects of the separated flow were not determined. It is believed that aerodynamic hysteresis does not affect the static stability and drag as strongly as it must effect dynamic stability; but no data were taken to support or deny that belief.

D. SHADOWGRAPHS

In both facilities, shadowgraphs were taken at zero angle of attack in all cases, and at $\alpha = 4°$ and/or $10°$ in most cases. These pictures were consulted often during the analysis, and support the conclusions drawn below. Selected photos, some of them accented by hand to alleviate poor visualization caused by low densities and reproduction losses, appear in Figures 9 through 12.

Reference 6 includes a discussion of the AEDC shadowgraph system and Reference 8 is a detailed narration of the design and performance of the MSFC system.

The shadowgraphs of Figures 9 - 12 show all four configurations at different Mach and Reynolds numbers, with and without boundary layer trips. They are discussed in detail in the next section.

SECTION III. RESULTS OF TESTS

In this section, the summary data derived from the tests are discussed. The data are compared with Newtonian predictions, and are supported by basic data (Refs. 1, 2), and the typical flow features illustrated by the shadowgraphs (Figs. 9 - 12). The discussion includes variations of stability derivatives and axial force coefficients with change in Mach and Reynolds numbers for the launch and high altitude configurations. Comparison of these two models yields the aerodynamic results of LES jettison. Study of abort-model data will show changes wrought by (but not during) freeing the Apollo in an emergency.

A. LAUNCH CONFIGURATION WITHOUT BOOSTER

Categorization of Summary Data. Figures 4a - 4d present the force and static stability characteristics of the launch configuration. The data all show a consistently flat variation with Mach number at both low and high speeds, but change suddenly near Mach 5. Above this point, the data can be grouped in two categories: laminar separation near the nose, and turbulent separation near the aft flare of the LES. The fairings are drawn according to the best estimate regarding applicability

to flight. Obviously, other fairings could be drawn, and there would be some argumentative support for them; however, the ones shown were chosen after careful consideration of the discussion presented in Appendix B. What seems like considerable data scatter is, for the most part, not. Nearly all trends and deviations from the "intuitively obvious" can be explained by theoretical arguments and/or published semi-empirical flow field studies. The key phenomena in the data behavior are transition, separation, and their causative mechanisms.

Review of Basic Data. The basic data (C_N, C_{mg}, C_{Af}) for these tests were reported in References 3 and 4. Their variations with α were identical to those of the older models (Refs. 1, 2) except for slight differences in magnitude. A short review of their behavior is in order; detailed plots are given in the references.

At Mach numbers between 1.9 and 4.5, all data were in the turbulent category. While magnitudes of the coefficients differed, their variational behavior was similar at all Mach numbers. This similarity was also true for all data in the laminar category, which applied to about half of the data bove Mach 4.5. In the turbulent cases, C_N and C_{mg} varied smoothly with α, without inflection points. The coefficients varied linearly up to $|\alpha| = 4°$, increased nonlinearly up to $\alpha = 14°$, and were again linear above $\alpha = 14°$. The forebody axial force coefficient, C_{Af}, peaked at $\alpha = 0°$, dropped off very slightly to a minimum at $\alpha = 4°$, then rose slowly, nonlinearly, and without inflection point past the $\alpha = 0°$ peak for the remainder of the angles of attack tested.

In the laminar cases, C_N and C_{mg} also varied linearly through $|\alpha| = 4°$, but with greater slope than in the turbulent cases. Between $\alpha = 4°$ and $\alpha = 6°$, the slope dropped off quickly, then went through an inflection point and behaved just as the turbulent cases did. C_{Af} was at a minimum, well below the turbulent value, at $\alpha = 0°$. It increased quickly up to $\alpha = 4°$, then leveled off and followed the turbulent behavior.

Nonlinearities in both laminar and turbulent data at intermediate angles of attack were a result of the formation, growth, and movement of a twin vortex system (Ref. 9). As α increased, the cross-flow Reynolds number increased; the vortices became unstable and alternately left the body. From this point on, separation was fully developed on the leeward side of the model, and C_N and C_{mg} varied linearly with α.

Flow Field at Zero Attitude. Locations of separation on the LES and reattachment on the CM correlate directly with magnitudes and trends of the data. At the low supersonic Mach numbers, the LES boundary layer is turbulent. It separates near the flare corner, reattaches to the flare, tries without success to expand around the flare base, and attaches to the command module near the tower mount. The shadowgraphs of Figure 9 show that reattachment on the CM is unsteady. The shock is strong but feathered. Overall, the shock is not a typical bow shock, but is of the conical,

attached type. Disregarding the unsteady fluctuations, it is seen that the shock does not begin to curve until expansive waves from the cone-cylinder shoulder reach it.

As the Mach number increases, the LES separation point moves forward. Earlier, it was stated that Mach number increase is an indirect cause of increased separation, through a reduction in total pressure and local Reynolds number behind the shock. A reduction in local Reynolds number also moves a transition region downstream. Thus, the LES boundary layer approaches complete laminarity as M increases. Shadowgraphs, many of which were not included in Figure 9 due to lack of space, showed that separation stayed close to the LES flare but then moved quickly upstream as Mach number increased. The rather quick movement upstream is believed to be associated with the onset of a completely laminar LES boundary layer.

Results of a classic investigation of Chapman, Kuehn, and Larson (Ref. 10) implied that the extent of separation depends strongly on Reynolds number only when the laminar shear layer (bounding the separated region) becomes turbulent before reattaching. Though disagreement is far from general, this implication is denied by the experimental studies of Gray (Ref. 11). Gray showed that the extent of purely laminar separation depends inversely on local Reynolds number for a fixed body length. This conclusion agrees qualitatively with the results presented here. Gray does not deny, however, that transition prior to reattachment will affect the upstream extent of separation. Thus, Chapman's point should be kept in mind when evaluating scale effects. One other point should be noted concurrently: laminar mixing layers are quite stable at high speeds. Transition may occur at reattachment, but generally occurs downstream.

As the separation locus moves upstream, the reattachment locus moves downstream on both the LES flare and the CM surface. Once separation reaches its maxmum, the LES flare is no longer hit by the shear layer, which then reattaches at the CM-SM shoulder. At this point, changes in stability and drag are greatest.

According to the theories of Chapman et al. (Ref. 10) and Korst (Ref. 12), reattachment on the upstream face of a flare or step is sometimes impossible because the reattachment angle is too large. In these cases, reattachment always occurs at the expansive shoulders. Besides placing a downstream limit of the CM-SM shoulder for the reattachment points (in absence of a large, steeply-angled flare further downstream), this thought may also explain the observed tenacity of the mixing layer in nicking the LES flare.

The upstream limit of separation is the LES cone-cylinder junction. First, laminar separations seldom propagate upstream past expansive corners. Second, the inviscid recompression just downstream of that corner gives an extra kick to separation at that point, aside from the effects of decreasing Re_D and increasing M.

Now that arguments have established the LES and CM cone-cylinder shoulders as the limits of separation at zero attitude, the data can be extrapolated above Mach 8. The LES leaves Saturn IB near Mach 6, but does not leave the Saturn V until above Mach 8. If the data of this report are to be applied to Saturn V (with appropriate changes in dimensional normalization), it is postulated that a simple extension of the fairings will give the desired data.

From the SM to the base, the flow is well-behaved. After the upstream chaos, the boundary layer is certainly turbulent. Any further separated regions would be local, caused by design protuberances. No separation was detected, nor was it expected, in the cylinder-frustrum compressive corner.

Flow Field at Non-Zero Attitude. The stability plots (Figs. 4a - 4c) were derived from the linear portions of the basic data, $-4° < \alpha < 4°$; the axial force graph (Fig. 4d) was cross-plotted from the basic data at $\alpha = 0°$. Thus, the term "non-zero attitude" primarily pertains to the range $-4° < \alpha < 4°$.

As the model pitches up a small amount, windward and leeward separation occur at different stations and the shear layer from the LES flare hits the CM asymmetrically. The locus of reattachment resembles an ellipse. Except on the CM cone, the load distributions on the windward and leeward meridians are similar in shape but different in magnitude. This basic flow picture is maintained as M increases (up to a point), causing very little change in $C_{N\alpha}$, $C_{mg\alpha}$ or CP/D. The variation in axial force coefficient at $\alpha = 0°$ is also quite slow, and is ascribed to the slow reduction in CM area which is under high pressure outside the reattachment locus. The shadowgraphs indicate that at $\alpha = 4°$ windward separation is close to the LES flare, while leeward separation occurs near the cone cylinder junction. At some point, indicated by the start of the rise of the stability curves, leeward reattachment on the CM reaches its aft limit, the shoulder, for small angle of attack. No shock is generated there. The windward and leeward load distributions are no longer similar in shape and become widely disparate in magnitude. The stability curves rise quickly and smoothly to a plateau regulated by fluid-dynamic restrictions on the volume of leeward separated flow. These jumps will definitely occur on any similar model and on the vehicle in flight. The main contention is not whether they occur, but when they occur. Since complete modeling is impossible, it must be asked whether partial modeling is adequate. Appendix B discusses this further.

Between Mach 4 and 6, which bounds the region of stability jumps, $C_{N\alpha}$ (Fig. 4a) rises over 70 per cent, $C_{mg\alpha}$ (Fig. 4b) rises 105 percent, and the center of pressure (Fig. 4c) moves forward, decreasing the stability by 0.6 caliber. Again, attention is called to the fact that C_{mg} is referred to the second stage gimbal station, while the center of pressure is referred to the booster gimbal station.

The axial force coefficient (Fig. 4d) drops by over 50 percent between Mach 5 and Mach 6. By comparing this figure with the stability-derivative plots it is seen

that in terms of Mach number the big change in axial force occurs after the big change in stability. It is also seen that the high Mach number, so-called turbulent data approach the laminar fairings on the stability plots, but do not on the axial force plot. This is not data scatter; it is the effect of angle of attack present in the stability derivatives but absent in the axial force plot. If a small angle of attack were held, the separated layer would hit the command module, and the axial force plot would just be a flat curve extending through the data labelled "AEDC, High Re." In this manner, the axial force data may be misleading. Vehicles tend to deviate from $\alpha = 0°$, and the fairing would underestimate their drag. Ballistic range tests would undoubtedly yield a considerable increase in drag from the faired hypersonic values.

Effectiveness of Trips in Inducing LES Transition. A good estimate can now be made regarding the performance of the boundary layer trips. Figures 4a and 4d will assist the estimation. Through Mach 4.45, trips and Reynolds number variation (the latter negligible at M = 4.45) did not affect the data.

The data clustered around Mach 5 is difficult to interpret. The triangle and flagged circle, and the diamond and flagged square are the only pairs of points where conditions were nearly identical in the two facilities. Their excellent agreement at a point where leeward separation is far forward in the former case and further aft in the latter confirms the belief that flow and freedom from turbulence are of the same high quality in both tunnels. It seems that the Nominal/Trip-Off condition did not provide a sufficiently high Re_D to delay separation compared with the Trajectory/Low condition (see also Fig. 3). When the trips were on the LES, the small increase from Trajectory/ Low to Nominal Re_D also had no effect; but these three points correspond to a delay in separation when compared with the three trip-off points. The differences are not large, but there is a definite indication that the trips were solely responsible for the separation delay and that the increase in Re_D had negligible influence. If nothing else, the trips distorted the boundary layer profiles enough to override the Trip-Off separation locus.

Looking (still at Mach 5) at the two High-Re_D points, one may observe that leeward separation was delayed whether the trip was off or on, a wholly expected occurrence at that Reynolds number. On the axial-force plot, the High Trip-On condition is indicative of a forward separation at $\alpha = 0°$. That point is attributed to experimental error, since a four percent increase in C_{A_f} would place it in the delayed-transition group.

At Mach 6, the Low Re_D points correspond to a greater-than-trajectory Reynolds number. From an increase in total-pressure-loss ratio across the bow shock, the surface Reynolds number would have decreased more than the 40 percent decrease in Re_D going from M = 5 to Mach 6. Here, addition of trips at Low Re_D

is not enough to delay separation; also, removal of trips does not move the High-Re_D separation forward. The difference in Reynolds number is dominant, and trips or lack of them cannot override this dominance at either condition.

At Mach 7, the Low Re_D has increased somewhat, and the High Re_D has dropped. The Trip-Off point corresponds to forward separation, but the Trip-On point indicates a delay. The difference in Re_D no longer dominates the separation.

At Mach 8, both Low and High Re_D have decreased enough that trips cannot delay leeward separation at small angle of attack. They can still delay zero-attitude separation somewhat at the High-Re_D condition. It is expected, though, that a small Mach number increase will bring the High-Re_D, Trip-On axial force point down to the laminar-separation fairing.

If a number of Mach number sweeps at various constant (or increasing, to account for total pressure loss) Reynolds numbers had been made, more definitive conclusions could have been reached about the conditions under which these trips were effective. In addition, the true effect of Reynolds number variation, as well as expected behavior at off-trajectory conditions, would have been defined. Economics and tunnel limitations forbade such a comprehensive study on this highly applied configuration. On the basis of the data available and Fig. 3, it was found that:

1. An increase of 50 percent in Re_D at M = 5 did not affect the data; an increase of 300 percent did. Addition of trips at the lower Reynolds numbers moved the separation aft.

2. The 600 percent increase of Re_D at M = 6 strongly affected the separation. Removal of trips did not amplify separation at High Re_D, and addition of trips did not depress it at Low Re_D.

3. The 300 percent increase of Re_D at M = 7 did not affect the data unless trips were used at the same time.

4. The use of trips at M = 8 had only a very small effect, even though there was a 300 percent increase in Re_D.

Finally, it is concluded that for this model and particular trip configuration under these test conditions, trips were usually effective in reducing separation.

B. HIGH ALTITUDE CONFIGURATION

By comparison with the launch configuration, this shape generates a placid flow field. The boundary layer sticks to the surface except for local spots at the design protuberances. It is likely to be a turbulent layer over most of the body

until the Mach number gets well into the hypersonic range. No separation was detected in the SM-LEM frustum corner. Boundary layer trips do not affect the data. Simple theories undoubtedly give good predictions of the coefficients, protuberances notwithstanding. The comparison with Newtonian impact theory (Ref. 13), calculated for a body without protuberances, was quite good.

Review of Basic Data. References 3 and 4 report the basic data obtained in these tests. The variation of C_N and C_{mg} with α was qualitatively the same over the whole Mach number range. The coefficients varied linearly to $|\alpha| = 5°$, increased their rates of change to $\alpha = 14°$, then varied linearly again. The only Reynolds number effect, not detected in the tests, would have been associated with turbulent (supersonic) or laminar (hypersonic) leeward separation over the whole model at high angles of attack.

The axial force coefficients exhibited a slight positive slope with α at $\alpha = 0°$ in the MSFC tests, but were perfectly flat in the AEDC tests. The nonzero MSFC slope may have been due to the asymmetric protuberances, which would have lost their effectiveness in the thicker boundary layer at hypersonic speeds; but the exact cause is not obvious. It may have been the result of an error in data reduction when gage and tare corrections were applied to the raw data. At any rate, the AEDC coefficients remained constant through $\alpha = 6°$, then increased gradually in both magnitude and rate of change with respect to α. At $\alpha = 20°$, the increase in C_{Af} was about 25 percent.

Discussion of Summary Data. Figure 5 presents the dependence of $C_{N\alpha}$, $C_{mg\alpha}$, CP/D, and C_{Af} on Mach and Reynolds number. A comparison of data and Newtonian predictions suggests that simple theory applies over a wide range of Mach number. Table II compares the Newtonian values with the hypersonic experimental results.

Between Mach 2 and Mach 8, the normal force slope, $C_{N\alpha}$, decreases only 15 percent and the decrease is almost linear. Newtonian theory predicts a slope 25 percent below the Mach 8 data. Protuberances were not included in the impact theory prediction; from area consideration, their contribution would be small. The only protuberances which could conceivably affect the normal force are the attitude control rockets and the long instrumentation tunnel. The small rockets would have no significant effect except through formation of a local high pressure zone if the boundary layer was turbulent. If the boundary layer was laminar, they might act as transition-provoking disturbances at higher angles of attack, thereby changing the leeward separation pattern. However, these data were taken from the low-α, linear portions of basic data. In this range, it is not felt that attitude control rockets would affect the derivatives. The instrumentation tunnel (on the S-IVB cylinder) would similarly affect a laminar-crossflow boundary layer. If the tunnel makes any force contribution at all, it is by being a stub-like surface having a small pressure differential across it at small angles of attack. The shadowgraphs of Figures 9-12

do not show the tunnel (see its location in Figure 2), but it is undoubtedly buried in the lower-speed strata of the boundary layer. Thus, the shock it generates is unlikely to be strong, and the lift-producing pressure differential across it is likely to be small.

The total change in the pitching moment slope, $C_{mg\alpha}$, is a 13 percent decrease, again nearly linear as M increases from 2 to 8. Impact theory is a little better here, only 13 percent below the Mach 8 data. Trips and increases in Reynolds number made no significant changes.

The center of pressure is nearly immobile as Mach number changes. The largest movement detected is 0.1 caliber (0.65 meter). Newtonian theory predicts a center of pressure 0.5 caliber (3.1 meters) ahead of the data prediction. Agreement is good.

The forebody axial force coefficient drops monotonically 25 percent between Mach 2 and 5, then levels off at a value of 0.297. Newtonian theory predicts a value of 0.245. In Reference 2, the Newtonian prediction was within one percent of the data between Mach 5 and 8 for a similar model. In the present case, the axial force coefficient predicted by Newtonian theory would have been increased by inclusion of protuberances in the calculation.

The constancy of axial force data above Mach 5 is an experimental confirmation of the Mach Number Independence Principle (Ref. 14). This principle effectively states that approximate flow field similarity can be attained for non-slender blunt bodies without simulating Mach number. Its lower Mach number limit of applicability varies with the body and the flow variable of interest. Here, it applies to pressures on a spherically blunted cone-cylinder-flare shape and two flat-nose shapes. The lower limit of applicability is Mach 5 for the high altitude configuration, and, as will be seen, somewhat lower for the abort shapes.

The shadowgraphs (Fig. 10) of the high altitude configuration indicate smooth, attached flow at zero angle of attack. The only separations visible are at and just behind the attitude control rockets. When the model is pitched up 10°, a typical reattachment shock and frustrum shock are discernible on the leeward side at Mach 4. Turbulence on the LEM and very weak shocks on the S-IVB protuberances indicate that lee separation is about to take charge over the whole body. At Mach 4.96, again at $\alpha = 10°$, lee separation has already taken effect. Trips do not affect the flow field. An AEDC shadowgraph at Low Re_D and M = 7.08 is included for interest. The Mach Number Independence Principle is thereby confirmed optically. The presence of trips is obvious from the compression, expansion, and recompression waves which they generate halfway along the Apollo cone.

C. JETTISON OF LAUNCH ESCAPE SYSTEM

In the case of the Saturn IB, the LES is jettisoned approximately 15 seconds after staging, which occurs at Mach 6-plus. In the Saturn V case, jettison occurs above Mach 8. The fairings from Figures 4 and 5 were redrawn and superposed in Figure 6. From these plots, the effects of LES jettison on the rest of the vehicle can be estimated.

Because the LES so completely dominates the forward flow field, fairly large changes in stability and drag characteristics were expected when the LES is jettisoned at higher Mach numbers. Below Mach 4.5, there is practically no change in the normal force derivative, stability derivative, or center of pressure. However, above Mach 4.5, where leeward separation and windward reattachment occur on the CM, the changes at jettison are large. $C_{N\alpha}$ decreases about 43 percent at Mach 6. At the same Mach number, $C_{mg\alpha}$ drops about 55 percent, and the center of pressure moves aft 0.75 caliber (4.9 meters).

It will be seen that abort produces comparable movements in the CP/D (0.6 → 1.1 caliber). In the LES-jettison case, however, the aft movement of the center of gravity would be considerably less than in the abort cases. Thus, the increase in stability margin would be greater in the LES-jettison case.

Of course, the transient effects of LES ignition and pluming are not considered. The tower-off data only apply when the main body is no longer affected by the plume, wake, or shock envelope of the LES rocket.

The axial force coefficient (Fig. 6d) increases at all Mach numbers when the LES is jettisoned. Before jettison, the LES creates a weaker nose shock and a cavity of low-momentum, recirculating flow on a portion of the CM. Therefore, some drag rise would be expected even at the lower Mach numbers. The increase in axial force at higher speeds is relatively larger. It must be remembered, however, that the pre-jettison curve applies only to angles of attack very close to zero. If jettison were to occur at hypersonic speed at a moderate vehicle attitude (for example, 4°), the pre-jettison axial force would be higher, the post-jettison axial force would be about the same as at $\alpha = 0°$, and the relative increase in axial force would be comparable to that of the lower Mach numbers.

D. ABORT WITH LAUNCH ESCAPE SYSTEM

Before staging, the LES is the most efficient means of pulling the Apollo away from the vehicle when the mission is threatened. If it is assumed an explosion is not the threat to the mission, the aerodynamic characteristics of the rest of the vehicle are of interest. These data would then be the initial conditions on a ballistic reentry problem to determine impact points.

In Figure 7, the fairings for the launch configuration (Fig. 4) have been superposed on the data and fairings for the LES-abort configuration. The changes which occur with abort are the changes which would be felt by the main body of the upper stage.

Review of Basic Data. The normal force and pitching moment coefficients varied with α in qualitatively the same manner over the whole Mach number range (Refs. 3, 4). Their variation was linear to $|\alpha| = 4°$, nonlinear with increasing rate to $\alpha = 14°$, and linear thereafter at about the same slope found in the tests of the high altitude configuration.

The axial force coefficients in the MSFC tests showed the same, small positive slopes through $\alpha = 0°$ as was reported for the high altitude configuration. In the AEDC (hypersonic) tests, C_{A_f} was constant to $\alpha = 6°$, then began rising slowly. At $\alpha = 20°$, C_{A_f} increased its value by only about 12 percent, which contrasts with the 25 percent increase reported for the high altitude configuration. Nearly all of this force is concentrated on the flat nose. A glance at the shadowgraphs shows that the bow shock hardly changes between $\alpha = 0°$ and $\alpha = 10°$. The force on the blunt nose would be nearly constant; therefore, the small changes in integrated axial force on the LEM frustum would be the prime movers in changing C_{A_f} with α.

Discussion of Summary Data. Figure 7 presents the LES-abort stability and axial force data, along with the fairings from Figure 4 representing the pre-abort characteristics. As a lifting body, this configuration is quite inefficient. Its lifting ability can be contrasted with that of the high altitude configuration, from which it differs only by absence of the Apollo. In both cases, the highest pressures are in the nose region. While the Apollo shock wave is weaker than the abort-shape wave, the cone surface contributes a healthy amount of normal force.

A second reason for reduction in lifting ability is the small-angle of attack boundary layer behavior at the nose. While the layer remained attached to the high altitude configuration as it flowed onto the SM, it could not negotiate the 90° expansion from the flat abort face to the SM cylinder. A flattened ring of separated flow is visible in the shadowgraphs, and it receives some local help in avoiding reattachment from the attitude control rockets. This ring of separated flow would still exist on the windward side at small angles of attack, drowning the windward attitude control rocket, and preventing a shock from forming a local high pressure zone at this point. The shadowgraphs at $\alpha = 10°$ show that at higher angles the windward separation is forced out of existence and the windward attitude control rocket makes its small contribution with a typical blunt-body shock.

Figures 7a – 7c show the variations of normal force and stability derivatives with Mach number; no consistent Reynolds number effect is visible. $C_{N\alpha}$ decreases

monotonically about 50 percent from Mach 2 through 8, leveling off on the way. The data agree closely with Newtonian impact theory from Mach 4.5 up (see Table II).

The pitching moment slope changes in the same manner, and proportionally by the same amount. The Newtonian prediction is less accurate than in the normal force case, but the magnitude of $C_{mg\alpha}$ is small.

The center of pressure is located near the LEM-frustum/S-IVB shoulder, and it is practically stationary with Mach number. The Newtonian prediction is off by one-half of a caliber, but part of this error is a result of random errors accumulated in dividing two small numbers. If $C_{N\alpha}$ and $C_{mg\alpha}$ data each has a random error of two percent, for example, the error in $CP/D = C_{mg\alpha}/C_{N\alpha}$ is about four percent.

The forebody axial force coefficient at $\alpha = 0°$ (Fig. 7d) is high and fairly constant over the whole Mach number range. The Newtonian prediction is about eight percent higher than the Mach 7 data, and would be a little farther off if the protuberance drag had been included. There is some doubt about the two data points at Mach 8. As will be seen, the same discrepancy occurs for the SM-abort model. It may be connected with errors in base pressure measurements.

When abort occurs, the trailing body feels widely varying changes in stability and axial force, depending on the Mach number. For example, at Mach 3 $C_{N\alpha}$ decreases 22 percent, $C_{mg\alpha}$ decreases 35 percent, the center of pressure moves aft 0.4 caliber (2.6 meters), and C_{Af} increases 109 percent. At Mach 6, $C_{N\alpha}$ decreases 70 percent, $C_{mg\alpha}$ decreases 79 percent, the center of pressure moves aft 1.2 calibers (7.7 meters), and C_{Af} increases 470 percent. The base figures for these percentages are the pre-abort data.

E.   ABORT WITH SERVICE MODULE

After the S-IVB engines ignite, the LES is dropped and the astronauts depend on the SM engine to get them out of trouble. This mode of escape can be used in the ascent trajectory or in earth orbit. If the vehicle is climbing toward orbit, the SM can place Apollo into a reentry path. Some consideration is being given to an abort into orbit; the restartable SM engine could then be fired for reentry at a more favorable time. The data taken on the SM-abort model can be used as initial conditions for stage reentry.

In Figure 8, the fairings for the high-altitude configuration (Fig. 5) have been superposed on the data and fairings for the SM-abort configuration. The data for the high-altitude shape were considerably more "well-behaved" than for the launch configuration. As a result, stability and axial force changes are less traumatic and less variable with Mach number than in the LES-abort case.

<u>Review of Basic Data</u>. As with the LES-abort model, the normal force and pitching moment coefficients varied with α in the same manner at all Mach numbers. They were linear to $|\alpha| = 4°$, nonlinear to $\alpha = 14°$, and linear thereafter. Other comments made in the previous section apply equally to SM-abort.

<u>Discussion of Summary Data</u>. Figure 8 presents the SM-abort stability and axial force data along with fairings from Figure 5, which represent the pre-abort characteristics. This configuration is also a poor lifting body, about half as efficient as the high altitude configuration.

The stagnation-region boundary layer must negotiate a sharp 81.4° turn. It cannot do so; the shadowgraphs (Fig. 12) again show a ring of separated flow just behind the intersection of the flat face and the LEM frustum. A conical shock emanates from the reattachment circle on the LEM. Note that no protuberance exists near this ring of separated flow. Both the ring and shock distort as α increases. At a 10° angle of attack, leeward reattachment occurs halfway back on the LEM flare.

The normal force and stability coefficients are given in Figures 8a - 8c. Reynolds number variation has no effect on the data. $C_{N\alpha}$ decreases by about 50 percent between Mach 2 and 8, with a slowing rate of decrease as M increases. As with the other abort configuration, Newtonian theory is an excellent predictor of the normal force slope.

The pitching moment slope decreases in a similar manner and by the same percentage. The Newtonian value is about 20 percent above the Mach 8 data, but its absolute error is not large.

The center of pressure is slightly behind the LEM frustum/S-IVB shoulder, and is practically stationary with Mach number. Impact theory yields a CP about 0.7 caliber forward of the experimentally determined position.

The forebody axial force coefficient at $\alpha = 0°$ is presented in Figure 8d. It is not constant as in the LES-abort case, but increases smoothly about 20 percent between Mach 2 and 8, approaching the Newtonian value of C_{A_f} ($\alpha = 0°$) = 0.75. As in the LES-abort case, the data takes a ten percent jump near Mach 8. No explanation for this jump is immediately obvious from flow field considerations, but errors in base pressure measurement at low dynamic pressures undoubtedly enter the problem.

Because the LES is not jettisoned until above Mach 6 in a typical Saturn IB trajectory, the SM-abort mode is not very interesting at the lower Mach numbers. The changes which occur in SM abort are practically invariant with Mach number, and are moderate in magnitude compared with those occurring in LES abort. At Mach 7.0, $C_{N\alpha}$ decreases 44 percent, $C_{mg\alpha}$ decreases 64 percent, the center of pressure moves aft 0.58 caliber (3.8 meters), and the axial force coefficient increases 132 percent.

SECTION IV. CONCLUSIONS

This report has shown that large changes in stability derivatives and axial force coefficient occur near Mach 5 for the Saturn IB/Apollo launch configuration's upper stage. Data below Mach 4 are characteristic of small turbulent separation at the LES flare, and data above Mach 6 are characteristic of large laminar separation over most of the LES. Changes with Mach number are gradual in these ranges. The large change near Mach 5 is associated with maximum forward movement of the separation locus. The movement causes the center of pressure to move forward, and lowers the axial force coefficient at $\alpha = 0°$ by 50 percent. Within certain ranges of Reynolds number at given Mach numbers, boundary layer trips are effective in delaying separation.

The high altitude configuration is not affected by trips or Reynolds number variation. Changes with Mach number are gradual. The center of pressure is nearly stationary from Mach 2 to Mach 8. Newtonian impact theory predicts stability derivatives and axial force coefficients quite well at hypersonic speeds.

When the LES is jettisoned below Mach 4.5, practically no change occurs in stability derivatives, and the axial force coefficient increases slightly. At higher Mach numbers, $C_{N\alpha}$ decreases over 40 percent, $C_{mg\alpha}$ decreases over 50 percent, the center of pressure moves aft 0.75 caliber, and the axial force increases about 150 percent at $\alpha = 0°$. These changes are stabilizing, and the gain in stability is greater than in either abort case.

Reynolds number does not affect either of the aborted configurations. $C_{N\alpha}$ and $C_{mg\alpha}$ decrease monotonically about 50 percent between Mach 2 and 8, keeping the center of pressure nearly stationary. The axial force coefficient is high and fairly constant with Mach number. Newtonian theory agrees quite well with the data.

When abort occurs in the launch configuration, the trailing body feels widely varying changes with Mach number. Below Mach 5, the CP moves aft less than 0.50 caliber, while above Mach 5, it moves aft over a full caliber. Drag increases by a factor of two to six, depending on the Mach number. Because LES jettison typically is programmed to occur near Mach 6, it is probable that this mode of abort would entail the less traumatic changes reported for lower Mach numbers.

When abort occurs in the high altitude configuration, stability and axial force changes are moderate and fairly constant with Mach number. This mode of abort would occur above Mach 6 if the standard trajectory were followed.

The fairings were drawn according to the best estimate of which data validly predicted full-scale characteristics. The estimates were based on consideration of the characteristics of hypersonic separation, compressible boundary layer behavior,

and the effects expected by violation of the rules of strict modeling. The only region of questionable validity is the immediate range of Mach number where large changes occur on the launch configuration. It is believed that the large changes will occur on the vehicle no later than at the Mach numbers where they are first predicted by data taken at trajectory conditions.

TABLE I

Average Test Section Reynolds Numbers

Mach No.	Facility	$Re_D \times 10^{-6}$	Re/meter $\times 10^{-6}$	Reynolds Number Designation
1.93	MSFC 14"	1.158	22.8	Nominal
2.99		.739	14.5	
3.48		.856	16.8	
4.00		1.120	22.0	
4.45		1.107	21.8	
4.96		.882	17.4	Nominal
4.00		1.423	28.0	Trajectory
4.45		1.138	22.4	
4.96	MSFC 14"	.582	11.46	Trajectory
4.97	AEDC "E"	.564	11.10	Low
5.99		.343	6.75	
7.08		.438	8.62	
7.76		.341	6.71	Low
5.03		2.64	52.0	High
6.11		2.16	42.6	
7.22		1.377	27.0	
8.05	AEDC "E"	1.042	20.5	High

TABLE II

Comparison of Newtonian Impact Theory* with Hypersonic Test Data

Model / Coefficient	$A_4^{8° 37'}$ Theory	$A_4^{8° 37'}$ Experiment	$A_4^{8° 37'} S_1$ Theory	$A_4^{8° 37'} S_1$ Experiment	$A_4^{8° 37'} S_1 C_1$ Theory	$A_4^{8° 37'} S_1 C_1$ Experiment
$C_{N\alpha}$ (deg.$^{-1}$)	0.0227	0.0220	0.0227	0.0200	0.0309	0.0410
$C_{mg\alpha}$ (deg.$^{-1}$)	0.0668	0.0550	0.0668	0.0450	0.104	0.118
$C_{Df} = C_{Af}$ ($\alpha=0°$)	0.748	0.700	0.748	0.685	0.247	0.298
$\left(\dfrac{CP}{D}\right)_{sta.\ 100}$	6.78	6.10	6.78	6.30	7.19	6.70

* Ref. 14
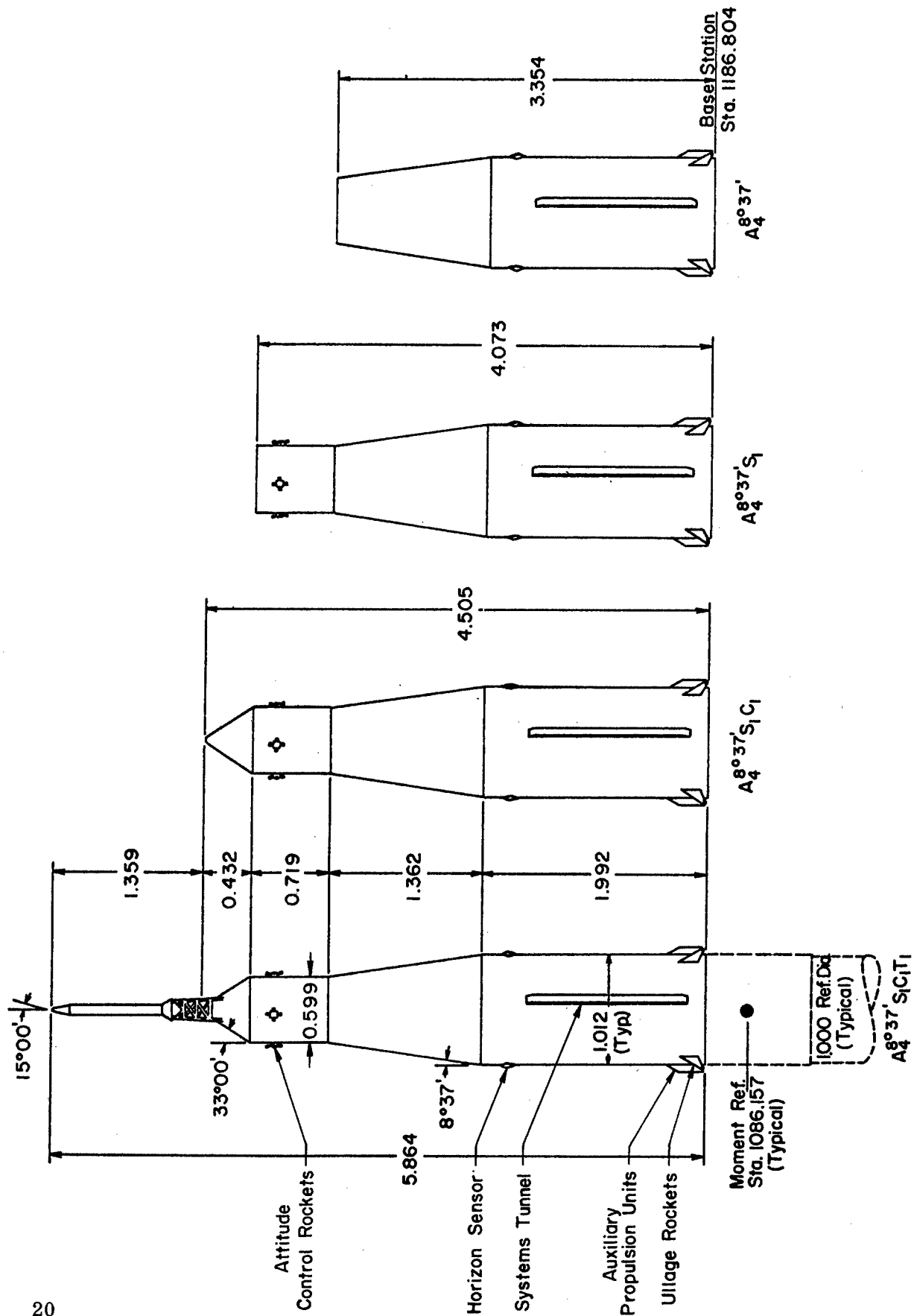
Figure 1. Geometric Details of the SATURN 1B Upper Stage Test Configurations
All dimensions in Calibers
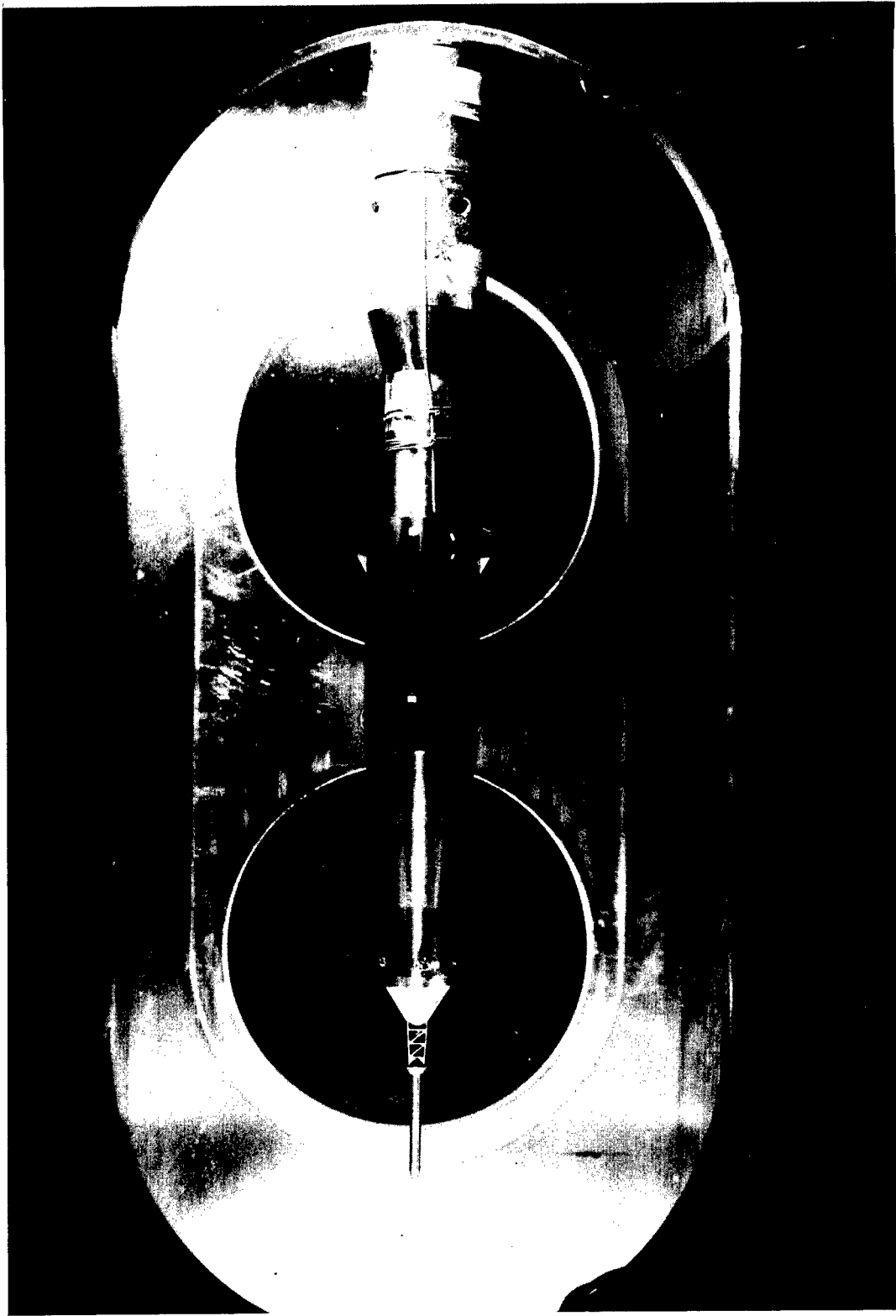
Figure 2. SATURN 1B Upper Stage Test Configuration $A_4^{8°37'} S_I C_I T_I t_3$ Sting - Mounted in the AEDC von Karman Facility Hypersonic Tunnel E.

21
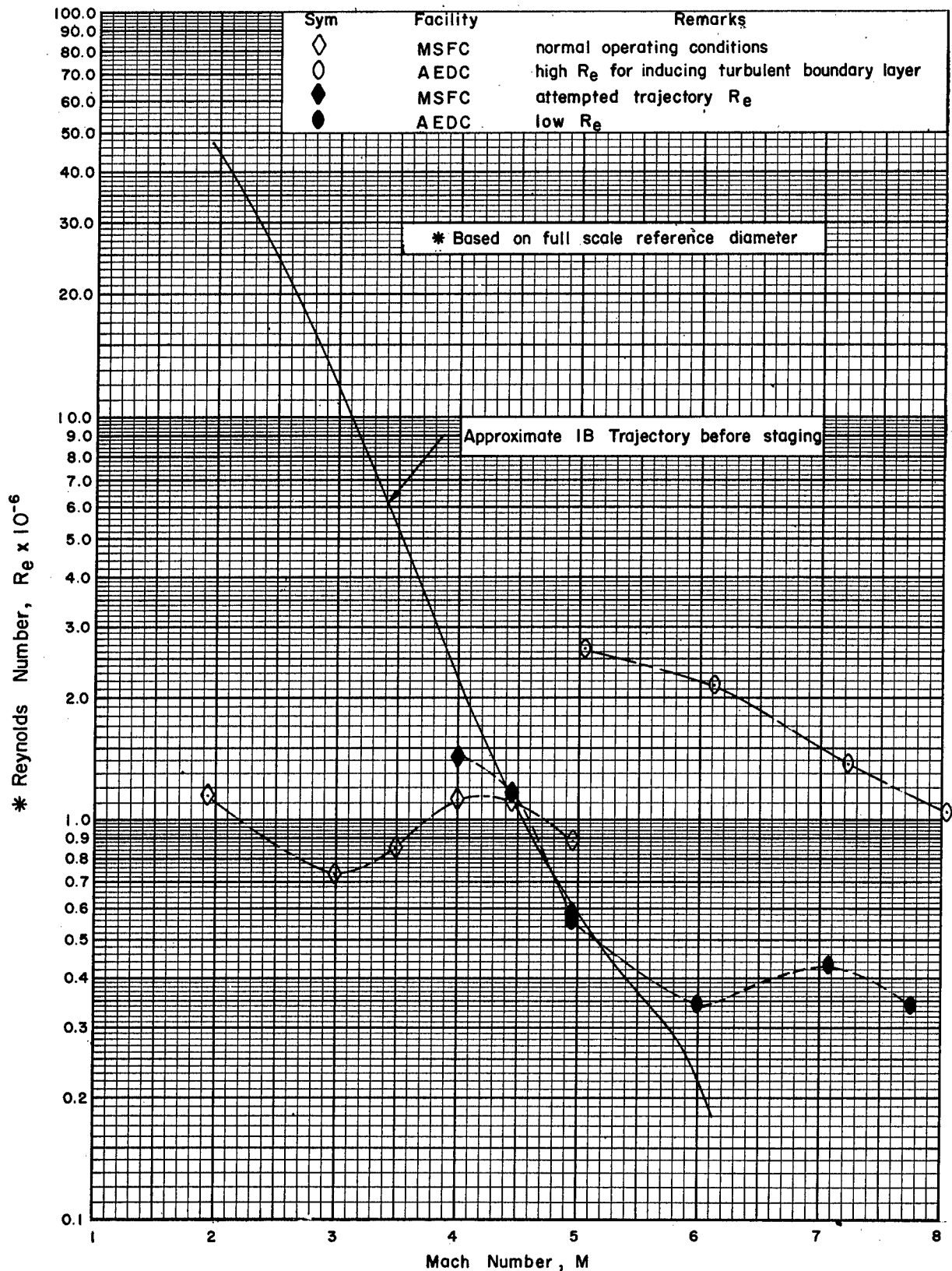
Figure 3. Comparison of Tunnel and Flight Conditions
for SATURN IB from Mach 1.93 – 8.05

(a) C_{N_α} , deg.$^{-1}$ vs Mach Number
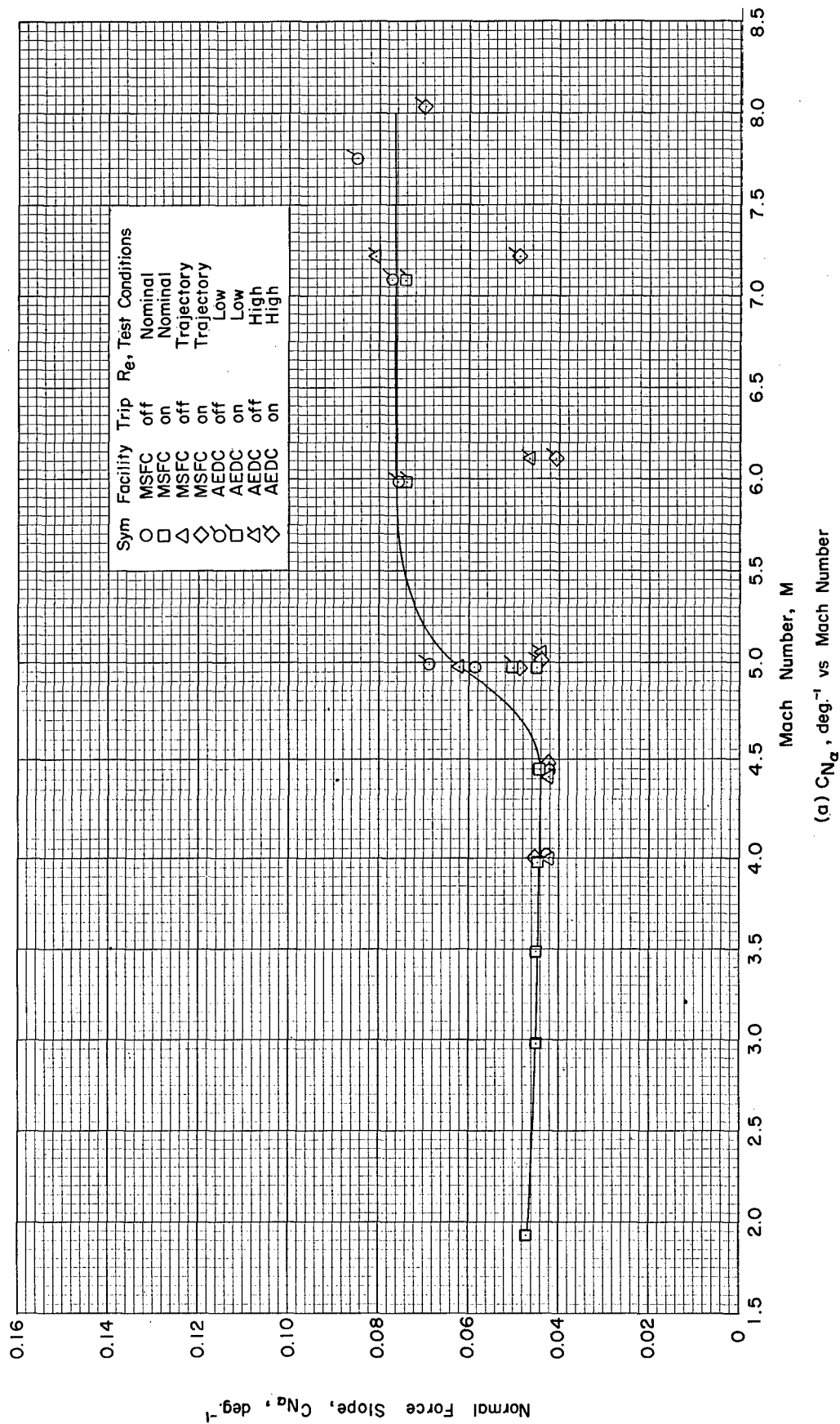
Figure 4. Effect of Reynolds Number and Trip on Model $A_4^{8°37'} S_1 C_1 T_1$ (Launch Configuration)

Mach Number, M

Normal Force Slope, C_{N_α}, deg.$^{-1}$

Sym	Facility	Trip	R_e, Test Conditions
○	MSFC	off	Nominal
□	MSFC	on	Nominal
△	MSFC	off	Trajectory
◇	MSFC	on	Trajectory
◷	AEDC	off	Low
⊡	AEDC	on	Low
◁	AEDC	off	High
◈	AEDC	on	High

23

(b) C_{mg_α}, deg.$^{-1}$ vs Mach Number

Figure 4. Continued

Mach Number, M

(c) CP/D vs Mach Number

Figure 4. Continued

Sym	Facility	Trip	Re, Test Conditions
○	MSFC	off	Nominal
□	MSFC	on	Nominal
△	MSFC	off	Trajectory
◇	MSFC	on	Trajectory
⬙	AEDC	off	Low
⬓	AEDC	on	Low
⬔	AEDC	off	High
◇	AEDC	on	High

CP/D, Calibers Forward of Vehicle Station 100, (Gimbal Station)

Moment Reference
Veh. Sta. 1086.157

25

8.5

8.0

7.5

7.0

6.5

6.0

5.5

5.0

4.5

4.0

3.5

3.0

2.5

2.0

1.5

Sym	Facility	Trip	Re, Test Conditions
○	MSFC	off	Nominal
□	MSFC	on	Nominal
△	MSFC	off	Trajectory
◇	MSFC	on	Trajectory
⬭	AEDC	off	Low
⬭	AEDC	on	Low
⬭	AEDC	off	High
◇	AEDC	on	High

Mach Number, M

(d) C_{A_f} ($\alpha = 0°$) vs Mach Number

Figure 4. Concluded

0.8

0.7

0.6

0.5

0.4

0.3

0.2

0.1

0

Forebody Axial Force Coefficient, C_{A_f}

Figure 5. Effect of Reynolds Number and Trip on Model $A_4^{8°37'}$ S_1 C_1 (High Altitude Configuration)

(a) C_{N_α}, deg. vs Mach Number

27
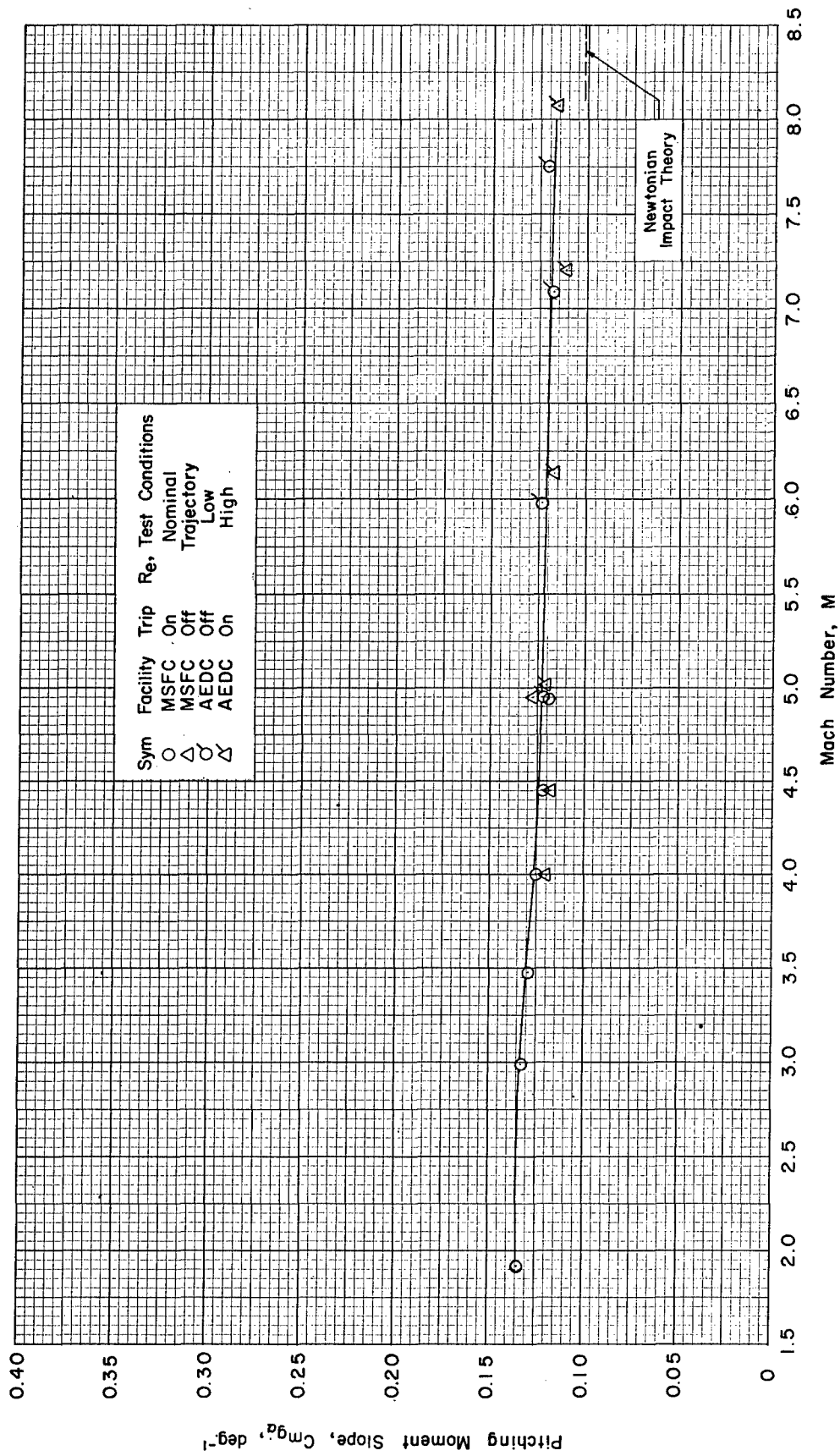
(b) $C_{m_{g_\alpha}}$, deg.$^{-1}$ vs Mach Number

Figure 5. Continued

Figure 5. Continued
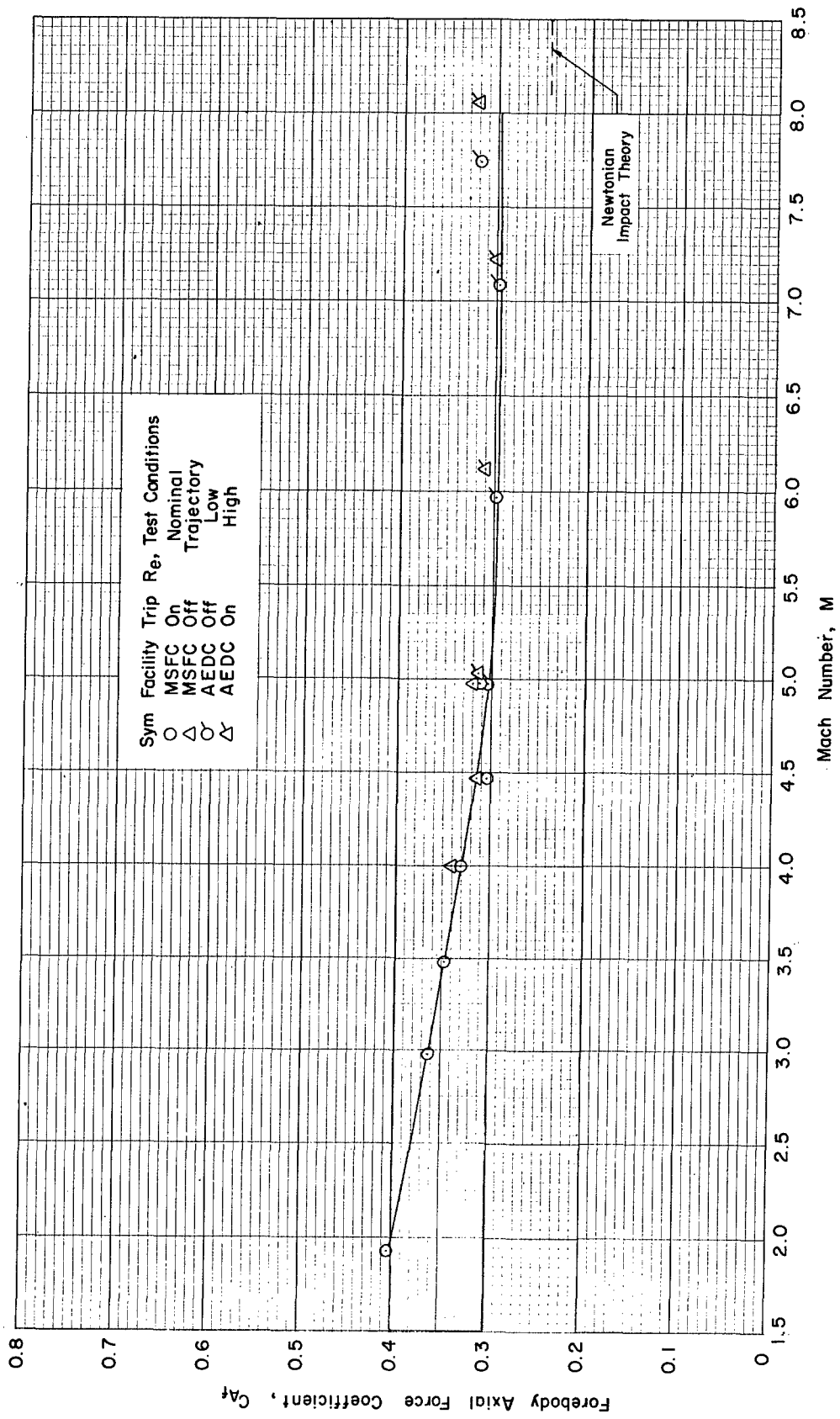
(c) CP/D vs Mach Number

(d) C_{A_f} ($\alpha = 0°$) vs Mach Number

Figure 5. Concluded
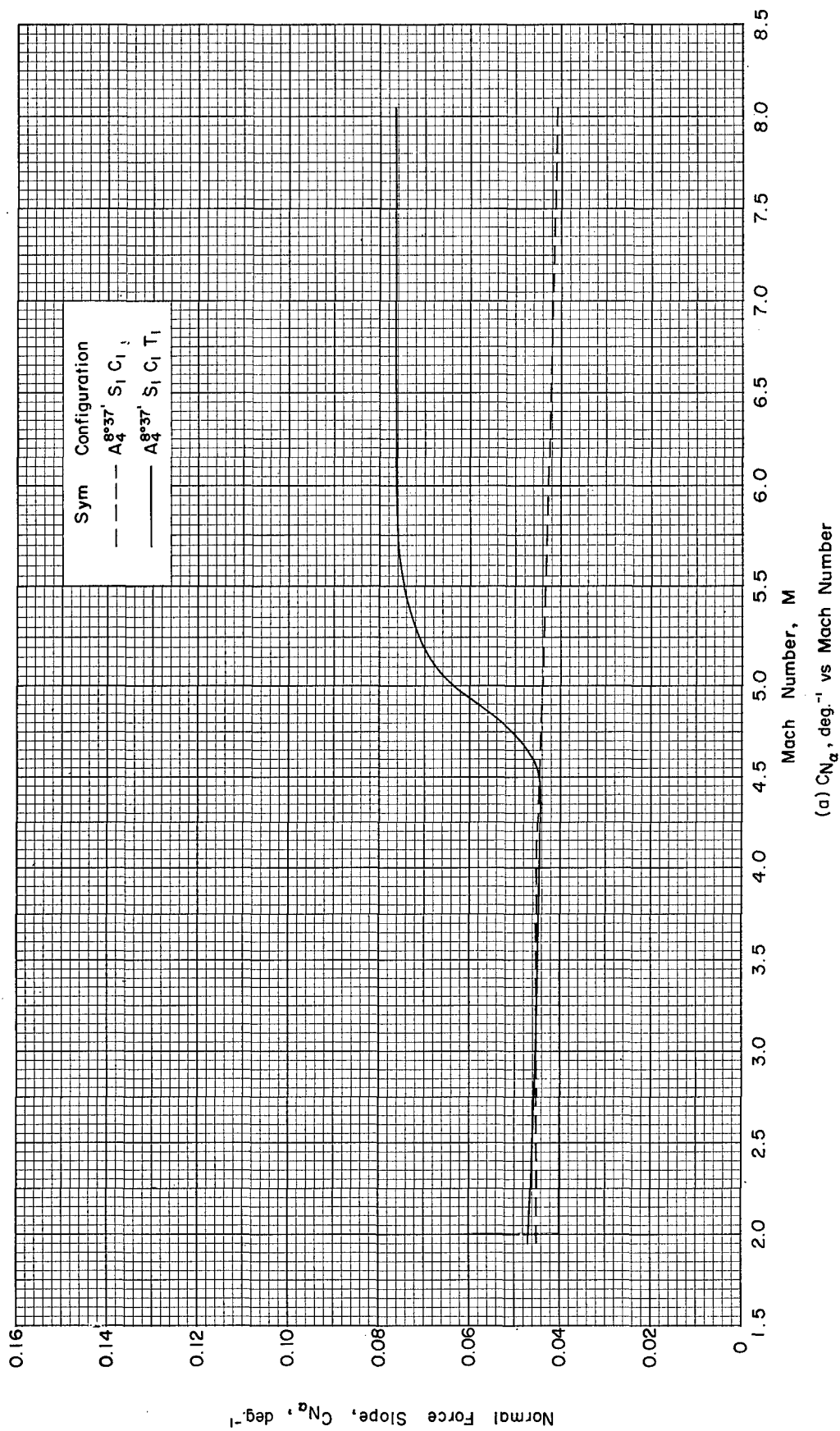
Figure 6. Effect of Jettison of the Launch Escape System

(a) C_{N_α}, deg.$^{-1}$ vs Mach Number

Mach Number, M

Normal Force Slope, C_{N_α}, deg.$^{-1}$

Sym	Configuration
$----$	$A_4^{8°37'}$ S_1 C_1
$-----$	$A_4^{8°37'}$ S_1 C_1 T_1

(b) C_{mg_α}, deg.$^{-1}$ vs Mach Number

Figure 6. Continued

Sym Configuration
— — — $A_4^{8°37'} S_i C_i$
———— $A_4^{8°37'} S_i C_i T_i$

Moment Reference
Veh. Sta. 1086.157

CP/D, Calibers Forward of Vehicle Station 100 (Gimbal Station)

Mach Number, M

(c) CP/D vs Mach Number

Figure 6. Continued

33
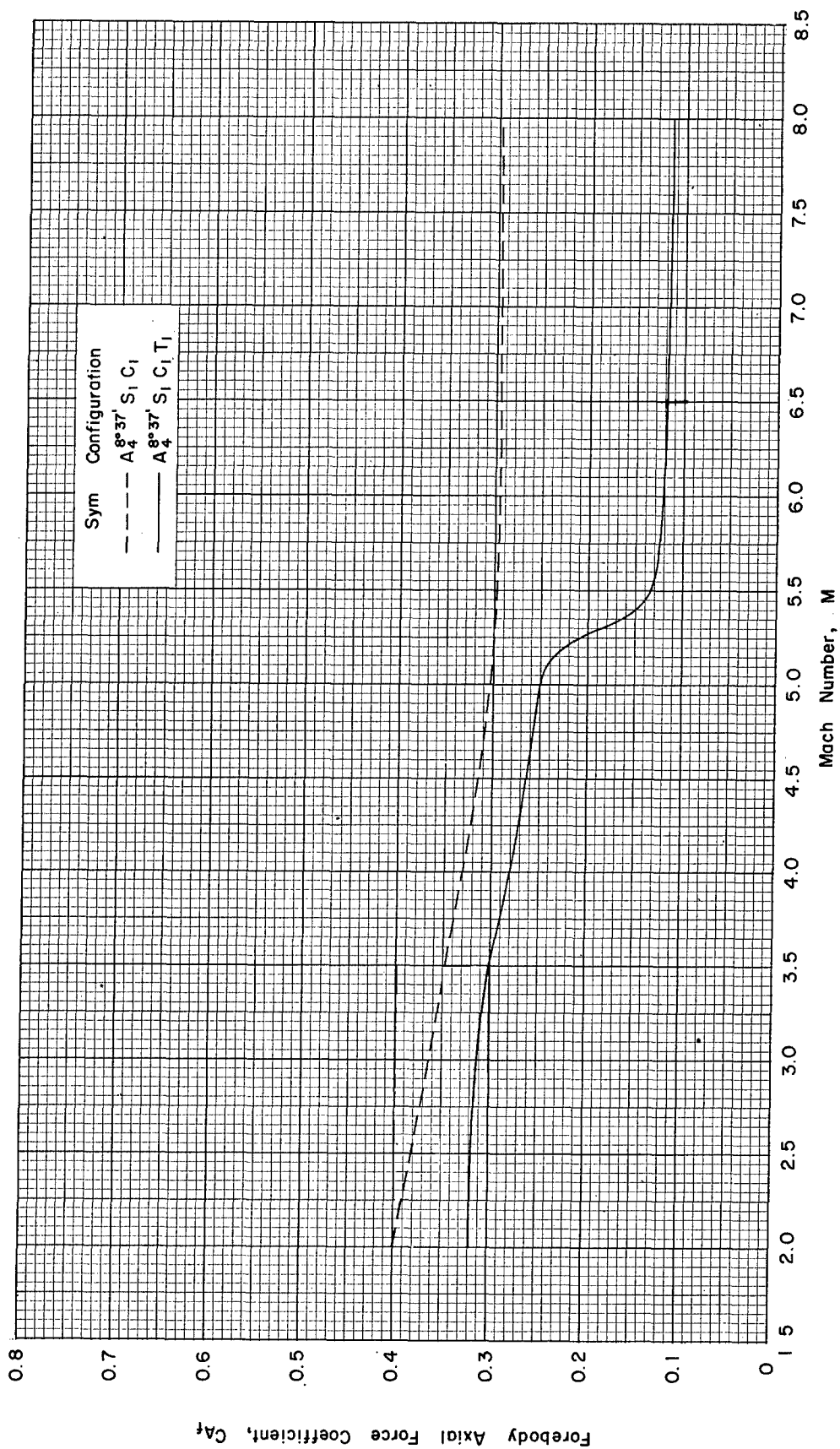
Mach Number, M

(d) C_{A_f} ($\alpha = 0°$) vs Mach Number

Figure 6. Concluded
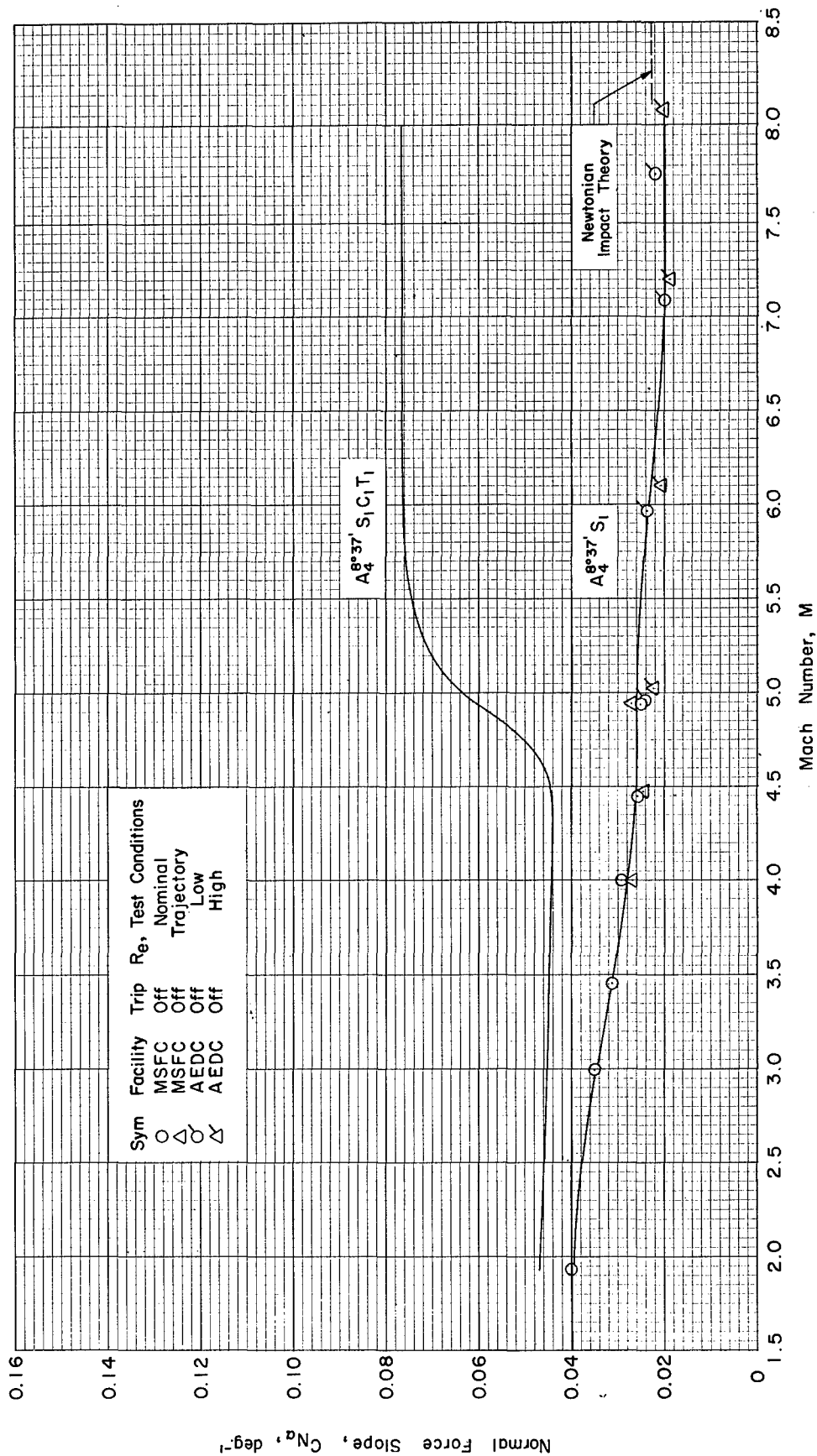
(a) C_{N_α}, deg.$^{-1}$ vs Mach Number

Figure 7. Effect of Launch Escape System Abort
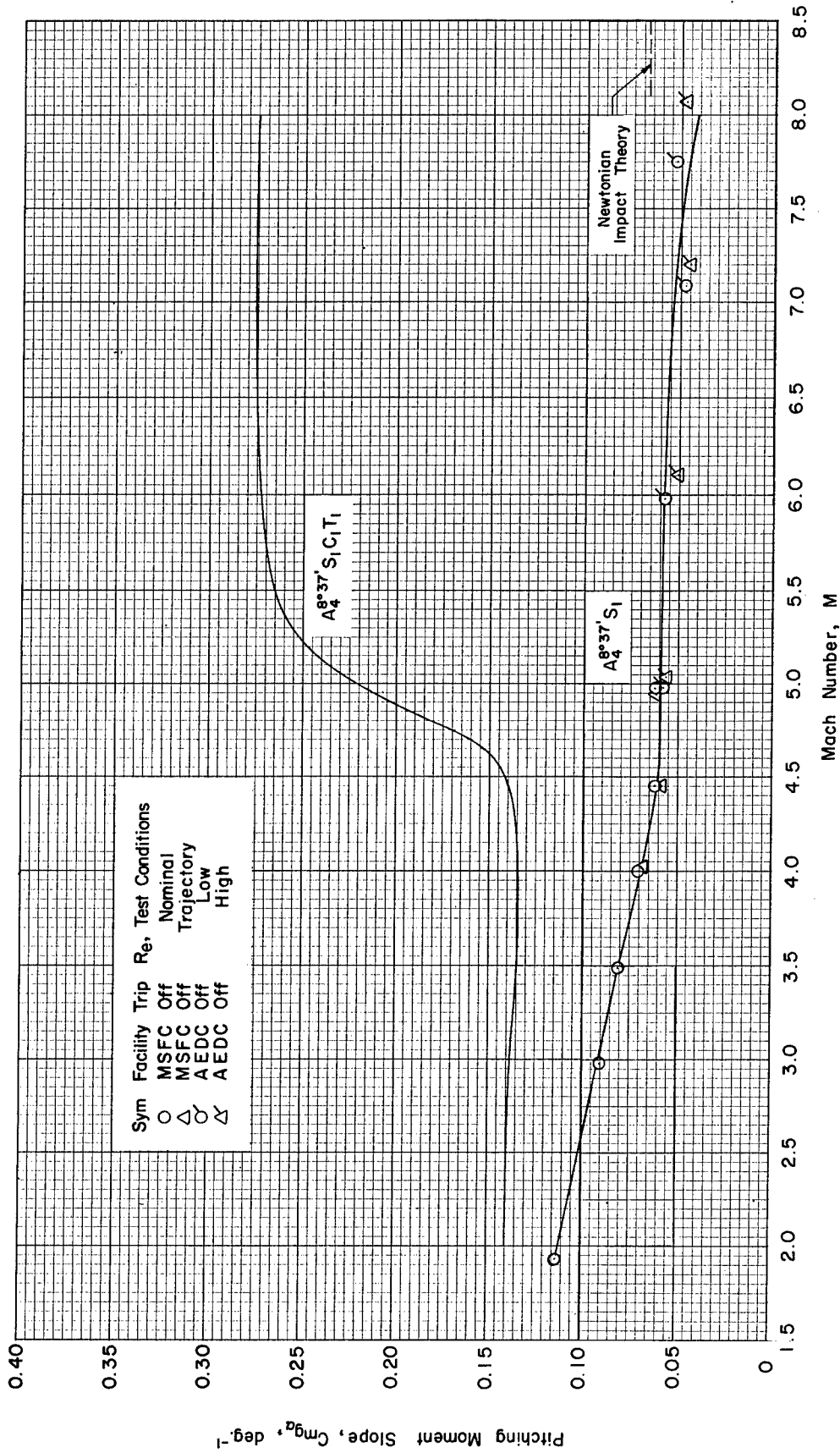
(b) $C_{m_{g_\alpha}}$, deg.$^{-1}$ vs Mach Number

Figure 7. Continued

(c) CP/D vs Mach Number

Figure 7.   Continued

37
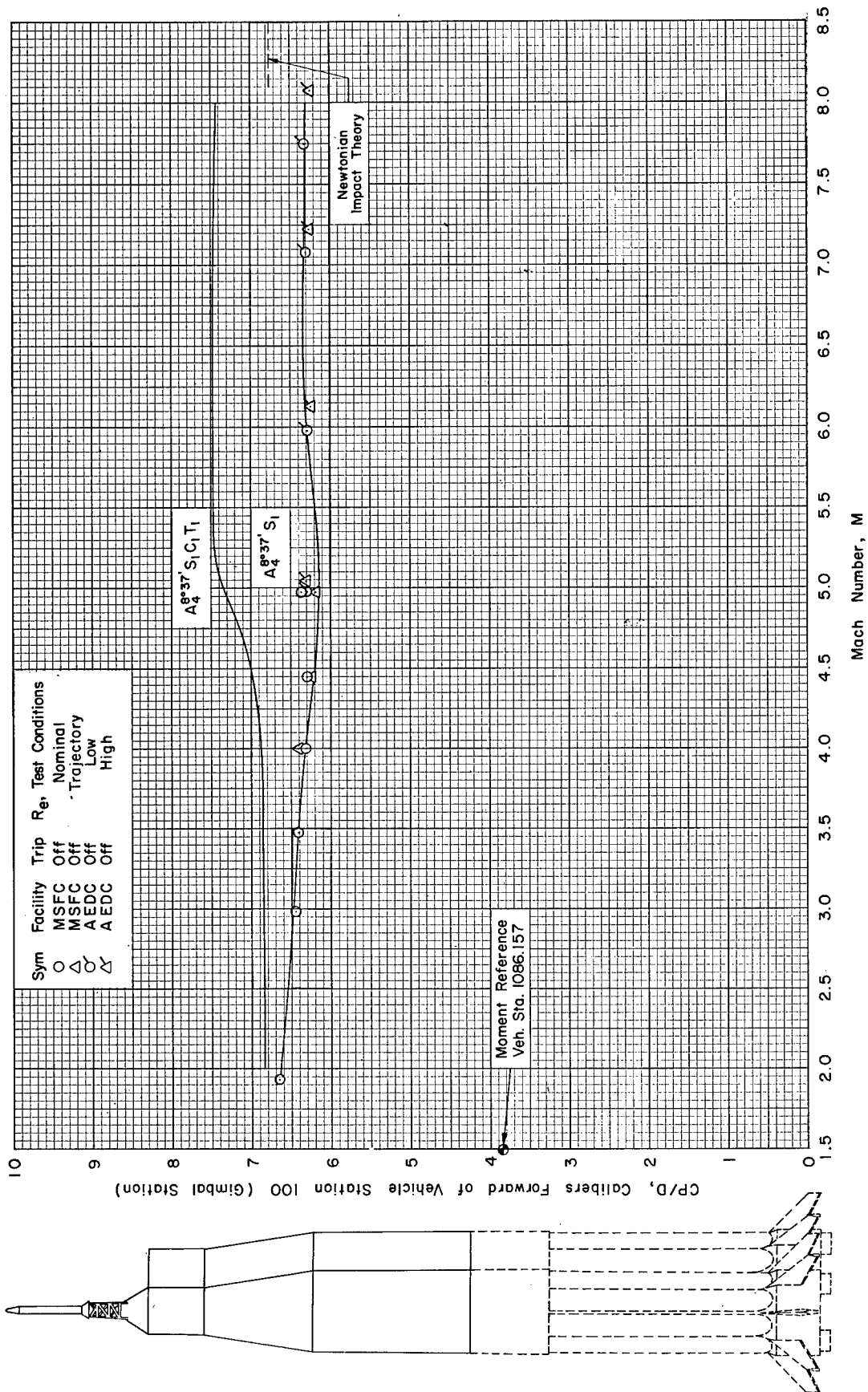
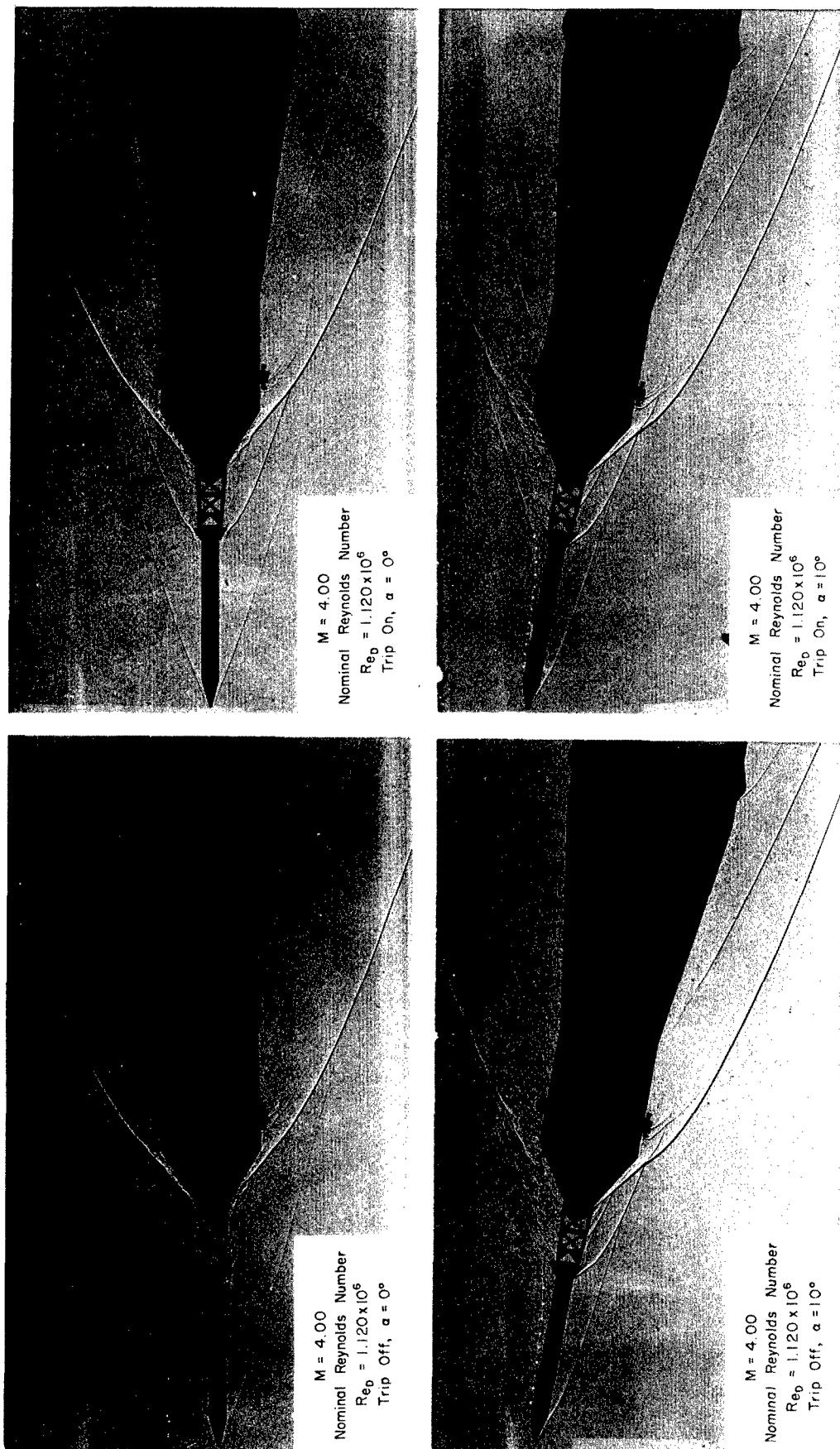(d) C_{A_f} ($\alpha = 0°$) vs. Mach Number
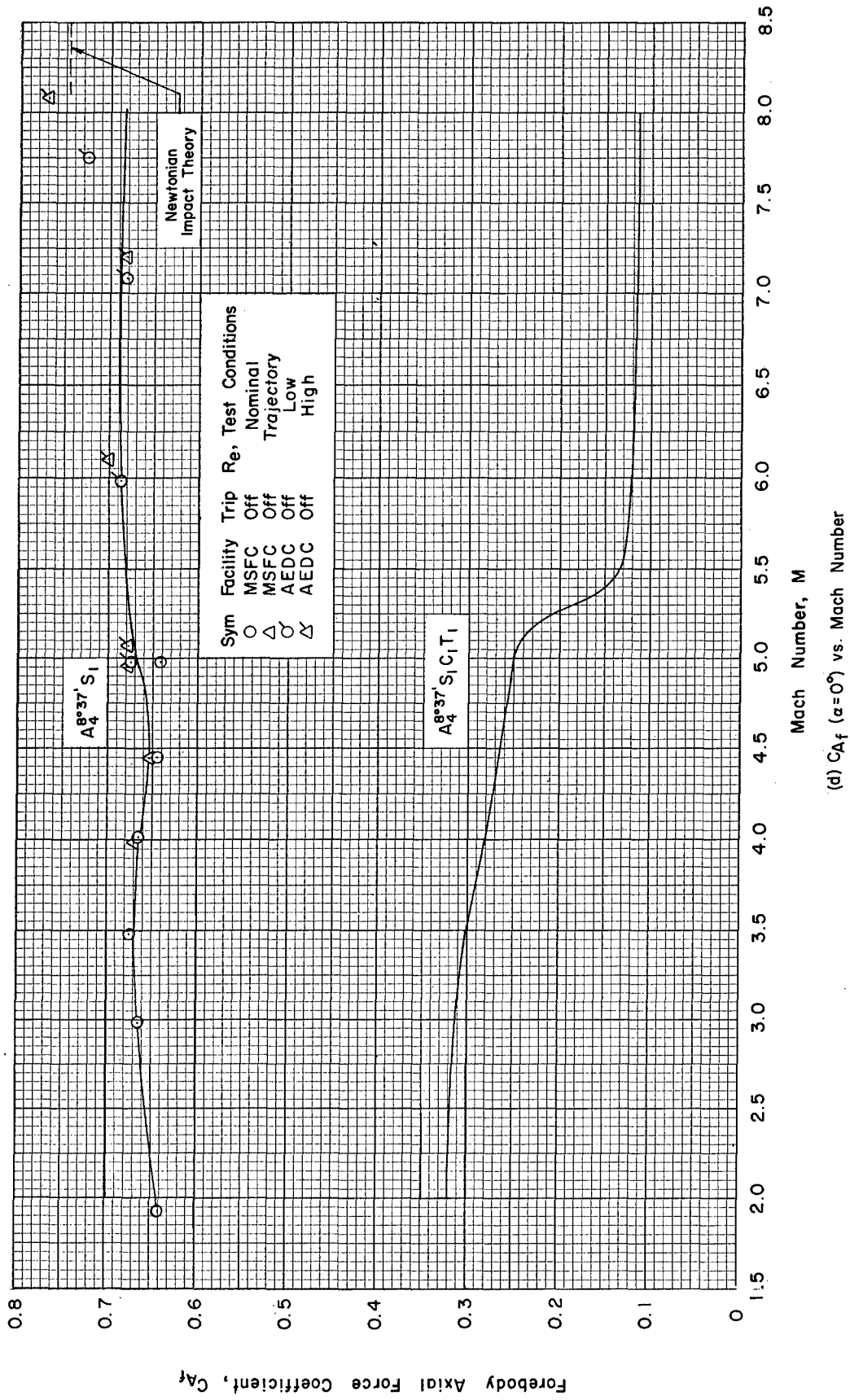
Figure 7. Concluded
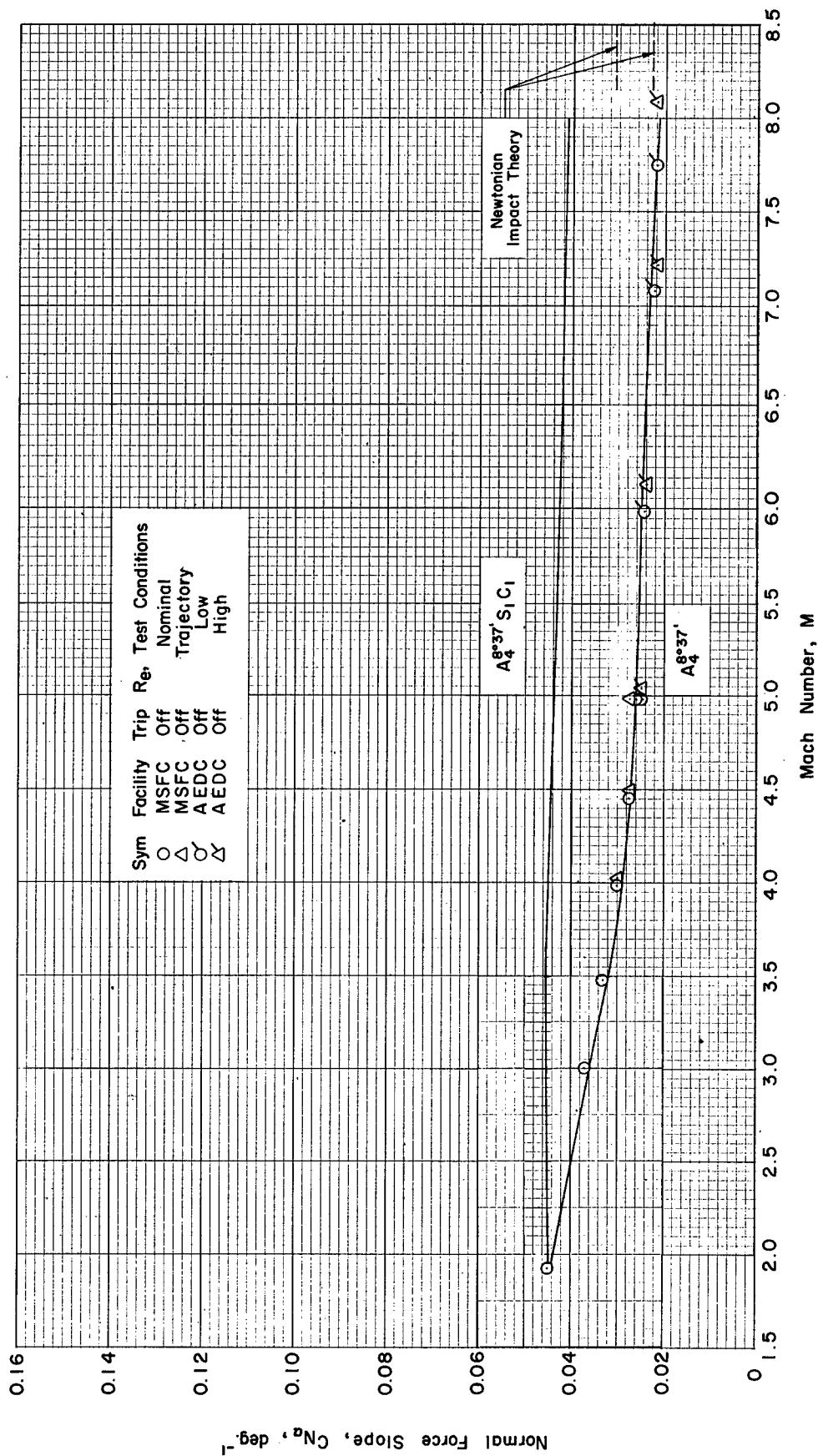
Mach Number, M

(a) C_{N_α}, deg.$^{-1}$ vs Mach Number

Figure 8. Effect of Service Module Abort

39
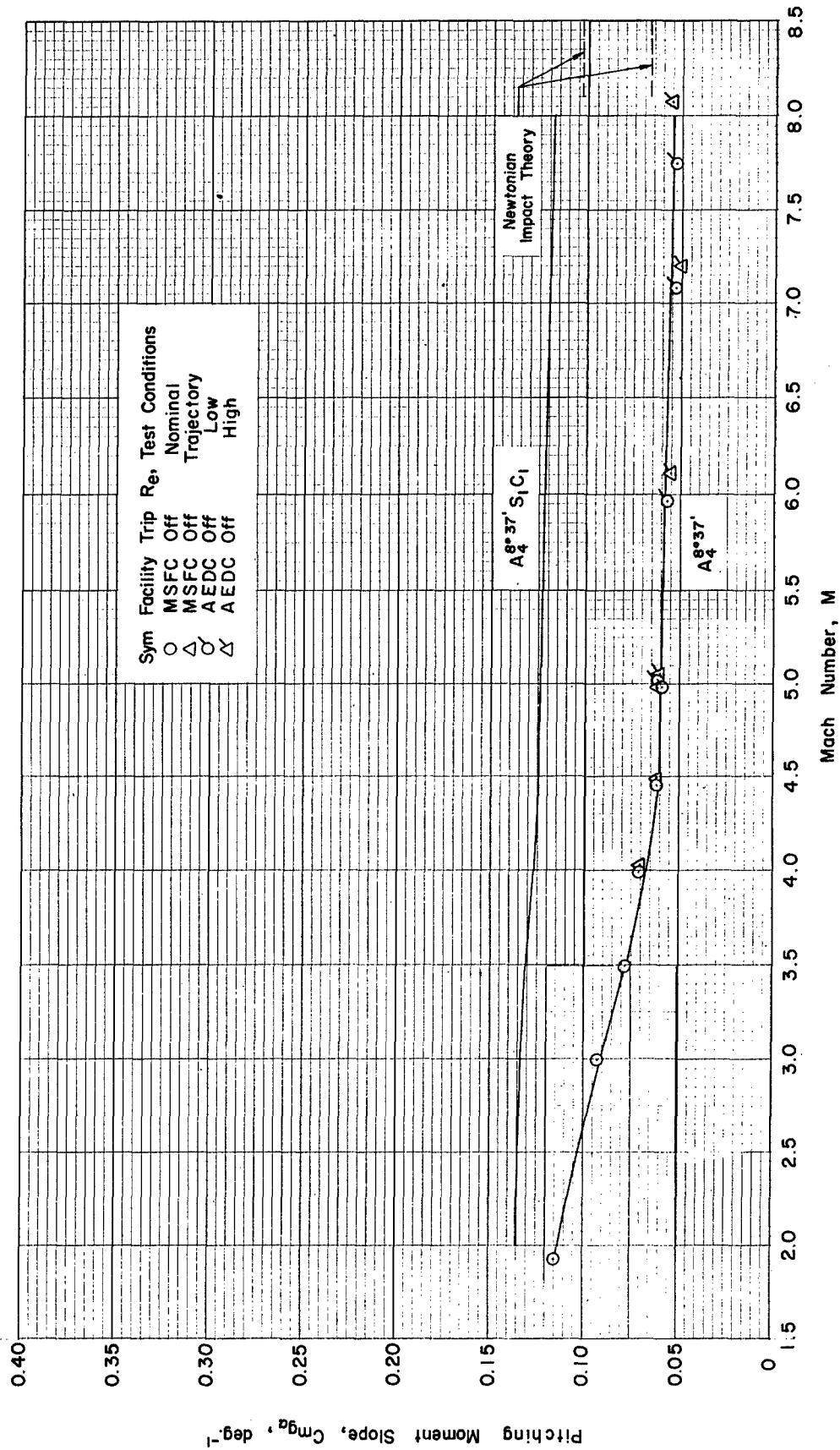
Mach Number, M

(b) Cm_{g_α}, deg.$^{-1}$ vs Mach Number
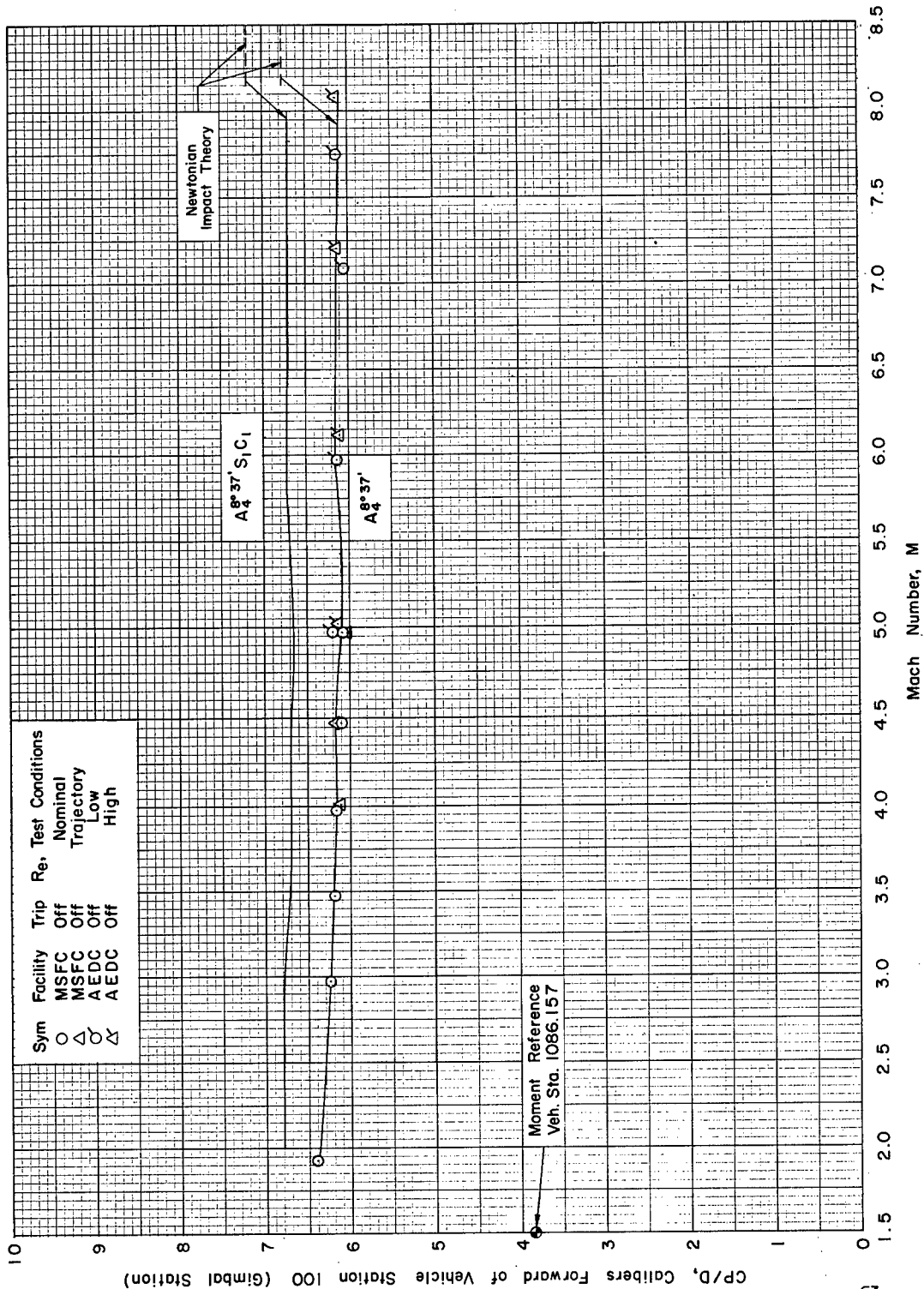
Figure 8. Continued

(c) CP/D vs Mach Number
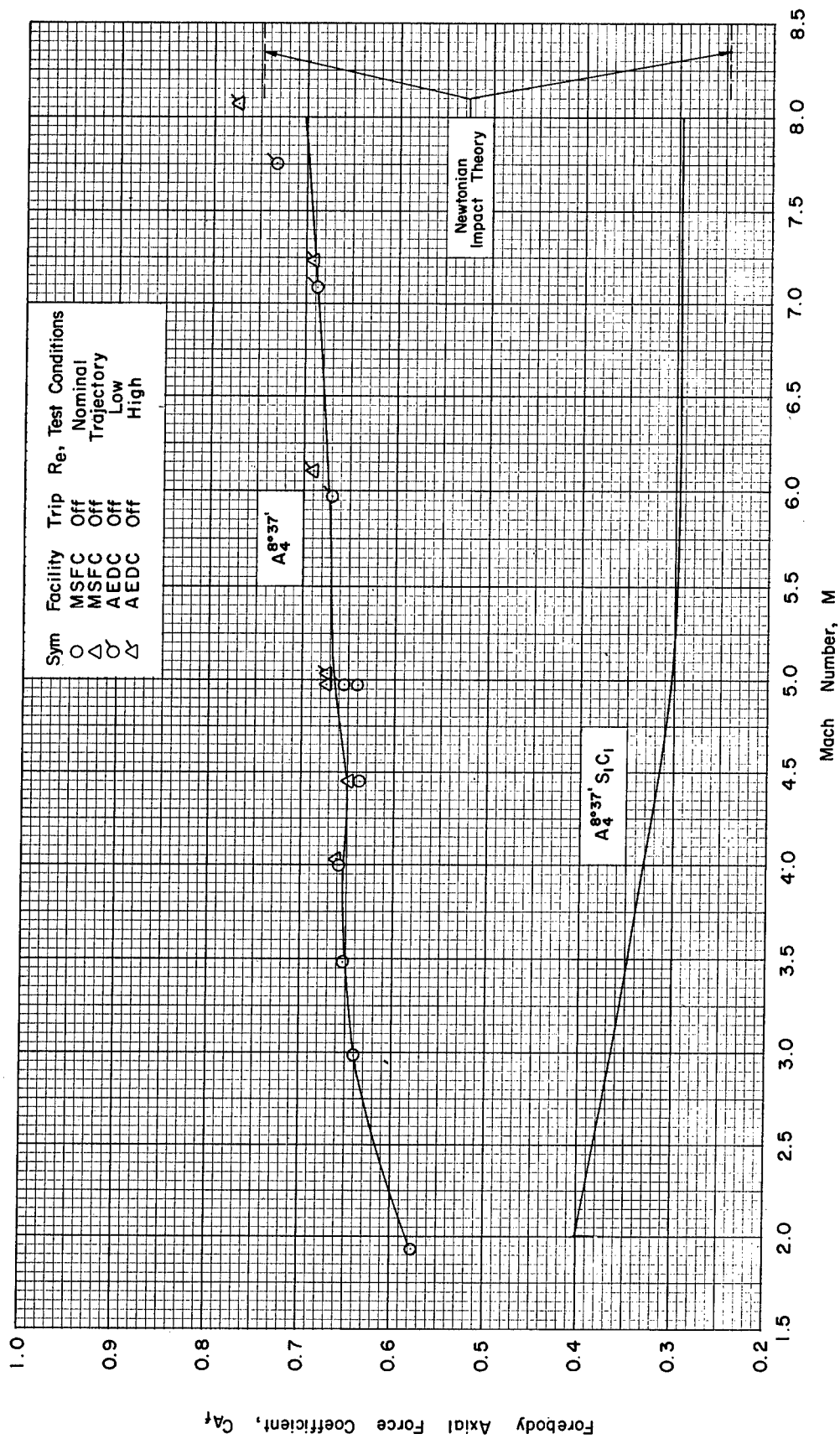
Figure 8. Continued

(d) CA_f ($\alpha=0°$) vs Mach Number

Figure 8. Concluded

42

M = 4.00
Nominal Reynolds Number
$Re_D = 1.120 \times 10^6$
Trip On, $a = 0°$

M = 4.00
Nominal Reynolds Number
$Re_D = 1.120 \times 10^6$
Trip On, $a = 10°$

M = 4.00
Nominal Reynolds Number
$Re_D = 1.120 \times 10^6$
Trip Off, $a = 0°$

M = 4.00
Nominal Reynolds Number
$Re_D = 1.120 \times 10^6$
Trip Off, $a = 10°$

Figure 9.   Selected Shadowgraphs of Launch Configuration

43

M = 4.96
Trajectory Reynolds Number
$Re_D = 0.582 \times 10^6$
Trip Off, $\alpha = 0°$

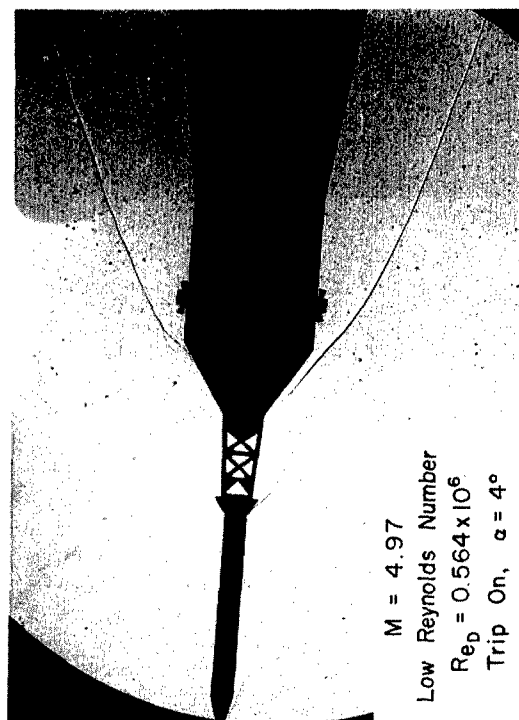

M = 4.96
Trajectory Reynolds Number
$Re_D = 0.582 \times 10^6$
Trip On, $\alpha = 0°$

Figure 9.   Launch Configuration (continued)

M = 4.96
Nominal Reynolds Number
$Re_D = 0.882 \times 10^6$
Trip On, $\alpha = 0°$

M = 4.96
Nominal Reynolds Number
$Re_D = 0.882 \times 10^6$
Trip Off, $\alpha = 0°$

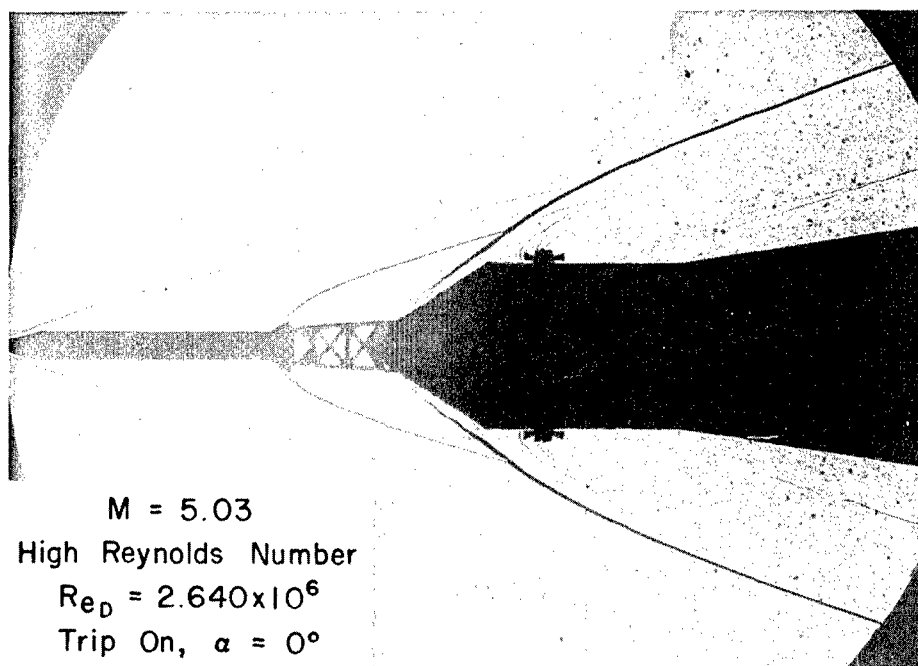M = 4.96
Nominal Reynolds Number
$Re_D = 0.882 \times 10^6$
Trip Off, $\alpha = 10°$

Figure 9. Launch Configuration (continued)

45

M = 4.97
Low Reynolds Number
Re_D = 0.564 x 10^6
Trip On, α = 0°

M = 4.97
Low Reynolds Number
Re_D = 0.564 x 10^6
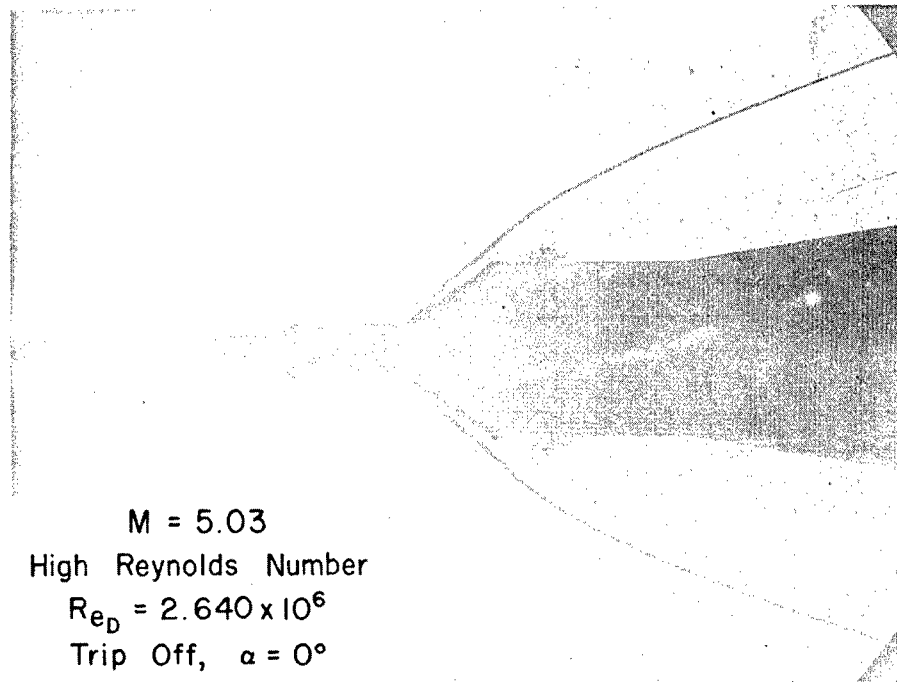Trip Off, α = 0°

M = 4.97
Low Reynolds Number
Re_D = 0.564 x 10^6
Trip On, α = 4°

Figure 9.   Launch Configuration (continued)

46

M = 5.03
High Reynolds Number
$Re_D = 2.640 \times 10^6$
Trip Off, $\alpha = 0°$

M = 5.03
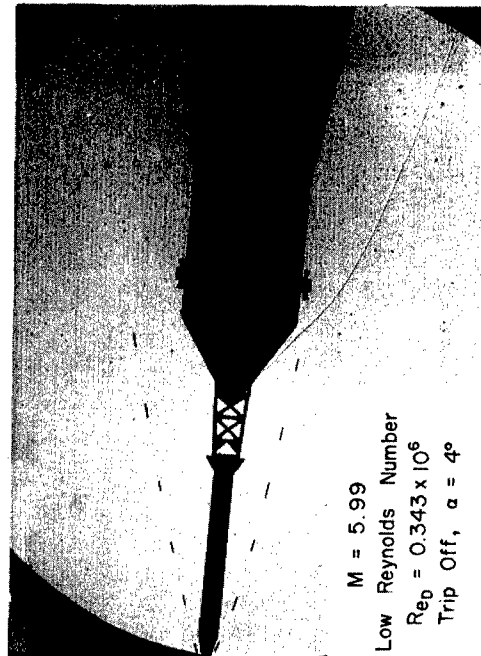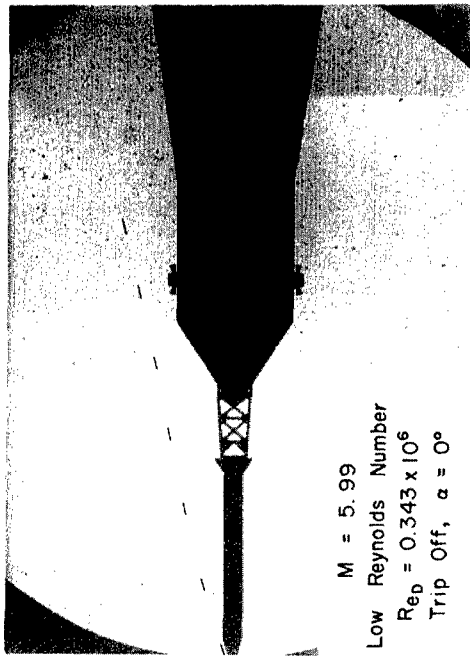High Reynolds Number
$Re_D = 2.640 \times 10^6$
Trip On, $\alpha = 0°$

Figure 9.   Launch Configuration (continued)

M = 5.99
Low Reynolds Number
Re_D = 0.343 x 10^6
Trip On, α = 0°

M = 5.99
Low Reynolds Number
Re_D = 0.343 x 10^6
Trip On, α = 4°

M = 5.99
Low Reynolds Number
Re_D = 0.343 x 10^6
Trip Off, α = 0°
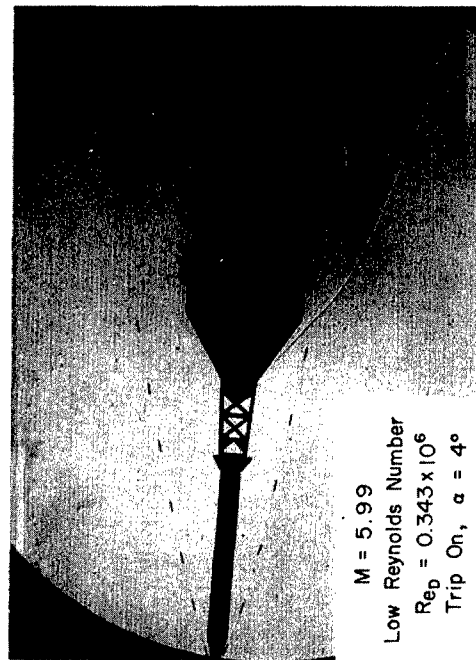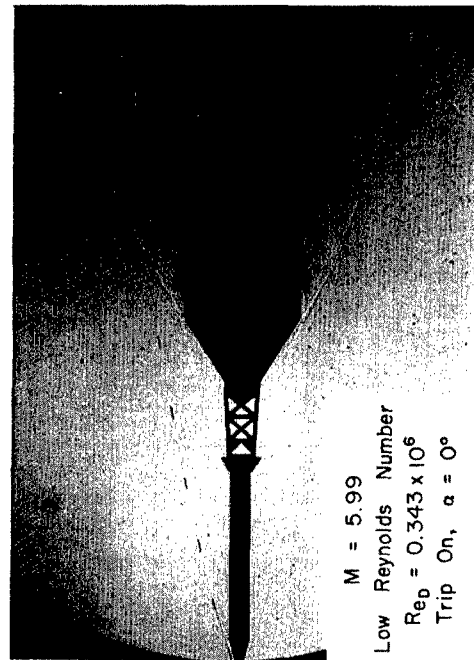
M = 5.99
Low Reynolds Number
Re_D = 0.343 x 10^6
Trip Off, α = 4°

Figure 9. Launch Configuration (continued)

M = 6.11
High Reynolds Number
$Re_D = 2.160 \times 10^6$
Trip On, $\alpha = 0°$

M = 7.08
Low Reynolds Number
$Re_D = 0.438 \times 10^6$
Trip On, $\alpha = 0°$

M = 6.11
High Reynolds Number
$Re_D = 2.160 \times 10^6$
Trip Off, $\alpha = 0°$
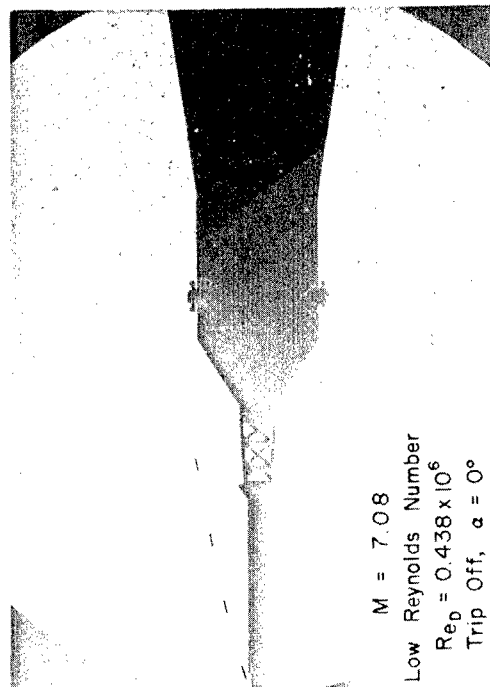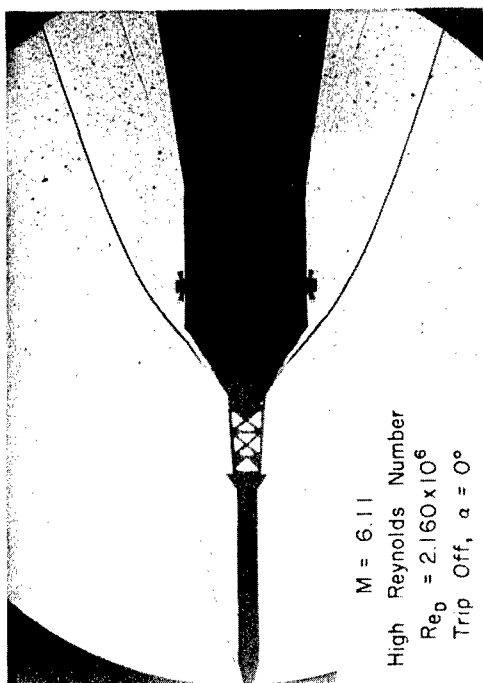
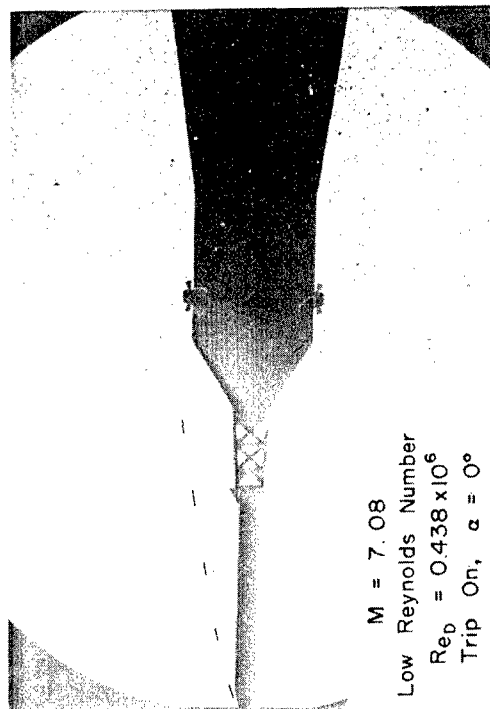M = 7.08
Low Reynolds Number
$Re_D = 0.438 \times 10^6$
Trip Off, $\alpha = 0°$

Figure 9.   Launch Configuration (continued)

49

M = 7.22
High Reynolds Number
$Re_D = 1.377 \times 10^6$
Trip On, $\alpha = 0°$

M = 8.05
High Reynolds Number
$Re_D = 1.042 \times 10^6$
Trip On, $\alpha = 0°$

M = 7.22
High Reynolds Number
$Re_D = 1.377 \times 10^6$
Trip Off, $\alpha = 0°$
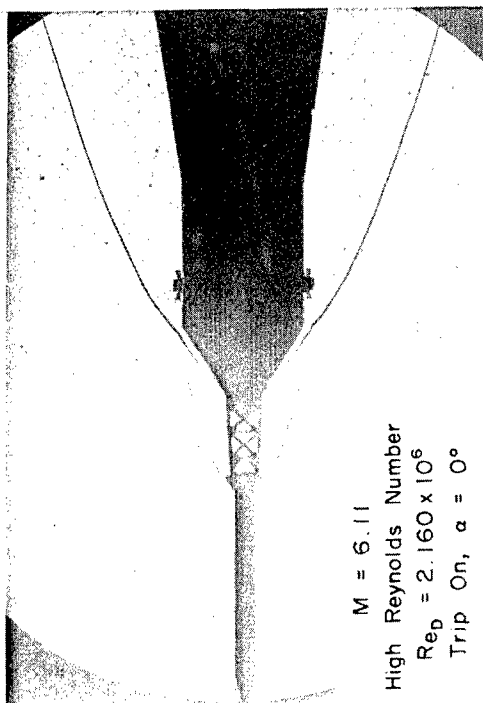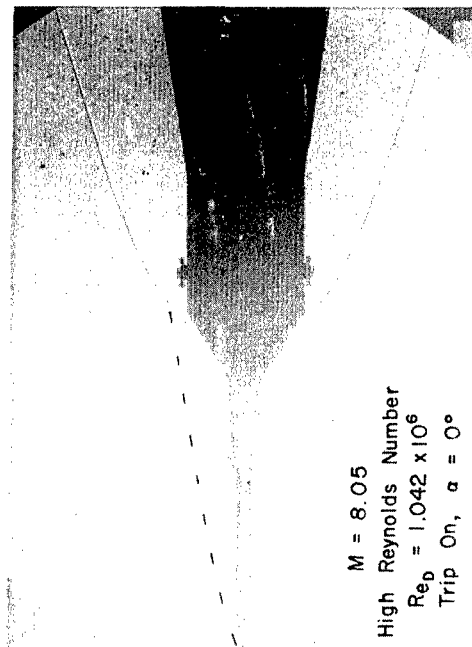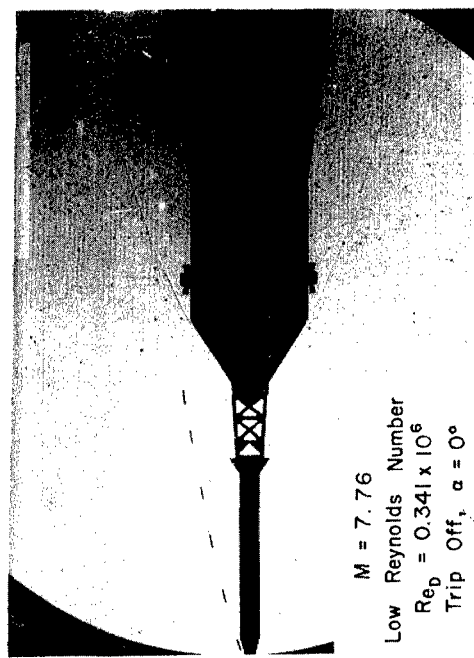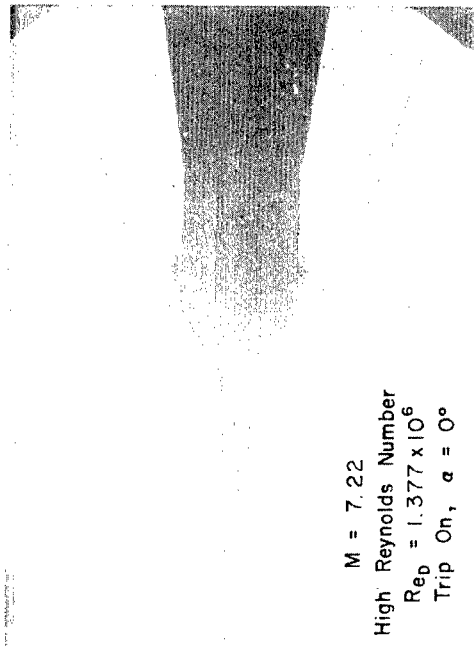
M = 7.76
Low Reynolds Number
$Re_D = 0.341 \times 10^6$
Trip Off, $\alpha = 0°$

Figure 9.   Launch Configuration (continued)

M = 4.00
Nominal Reynolds Number
$Re_D = 1.120 \times 10^6$
Trip On, $\alpha = 0°$

M = 4.96
Trajectory Reynolds Number
$Re_D = 0.582 \times 10^6$
Trip Off, $\alpha = 0$

M = 4.00
Nominal Reynolds Number
$Re_D = 1.120 \times 10^6$
Trip On, $\alpha = 10°$

Figure 10. Selected Shadowgraphs of High Altitude Configuration

51

M = 7.08
Low Reynolds Number
$Re_D = 0.438 \times 10^6$
Trip Off, $a = 0°$

M = 4.96
Nominal Reynolds Number
$Re_D = 0.882 \times 10^6$
Trip On, $a = 0°$

M = 4.96
Nominal Reynolds Number
$Re_D = 0.882 \times 10^6$
Trip On, $a = 10°$
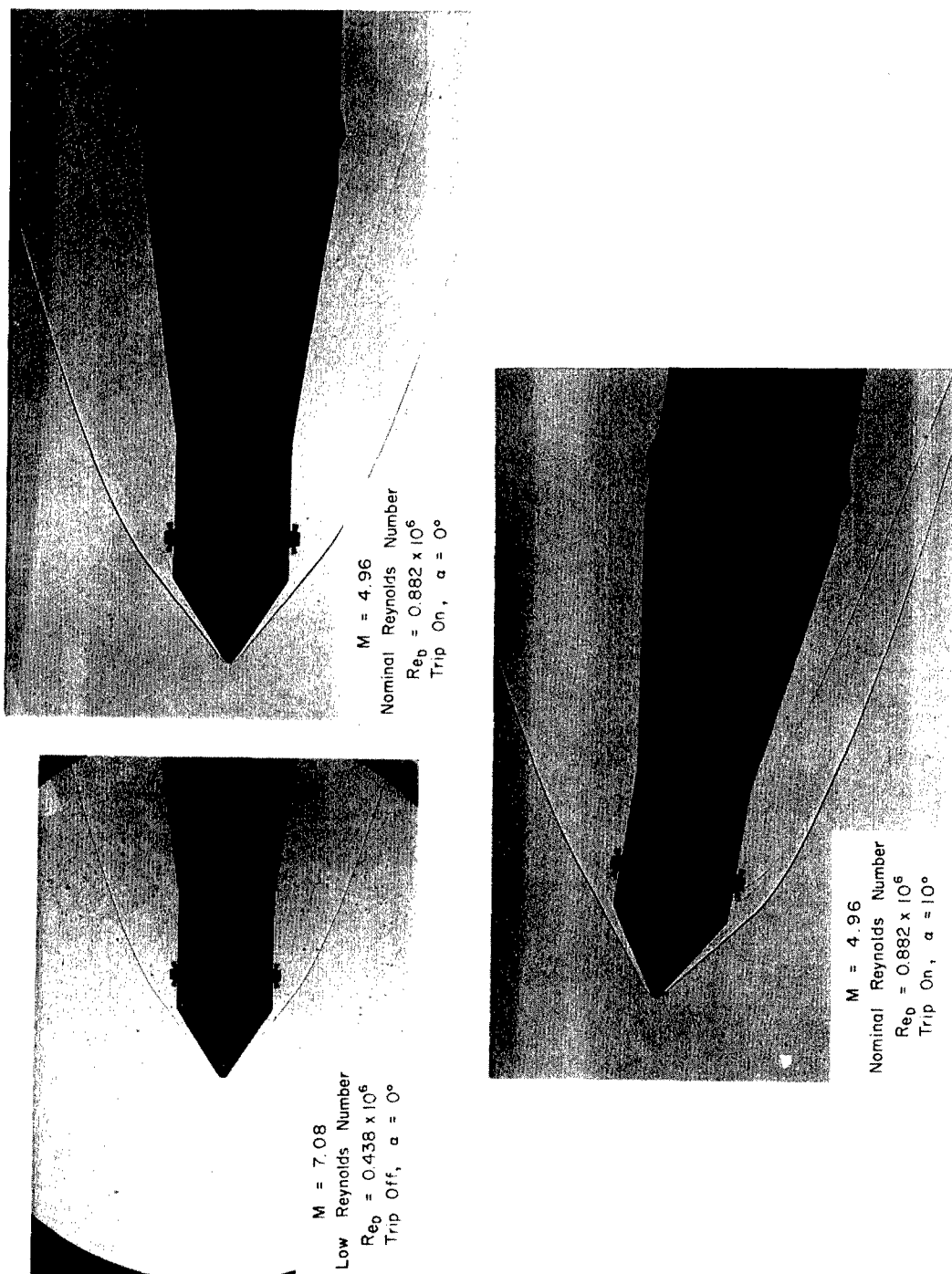
Figure 10.   High Altitude Configuration (concluded)

M = 4.00
Nominal Reynolds Number
$Re_D = 1.120 \times 10^6$
$\alpha = 0°$

M = 4.00
Nominal Reynolds Number
$Re_D = 1.120 \times 10^6$
$\alpha = 10°$
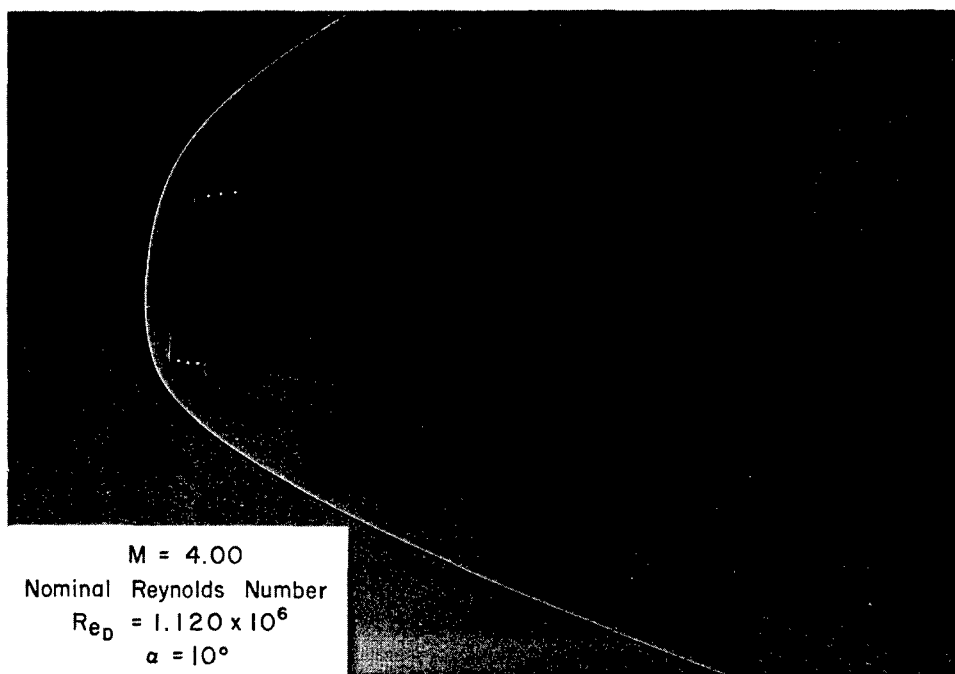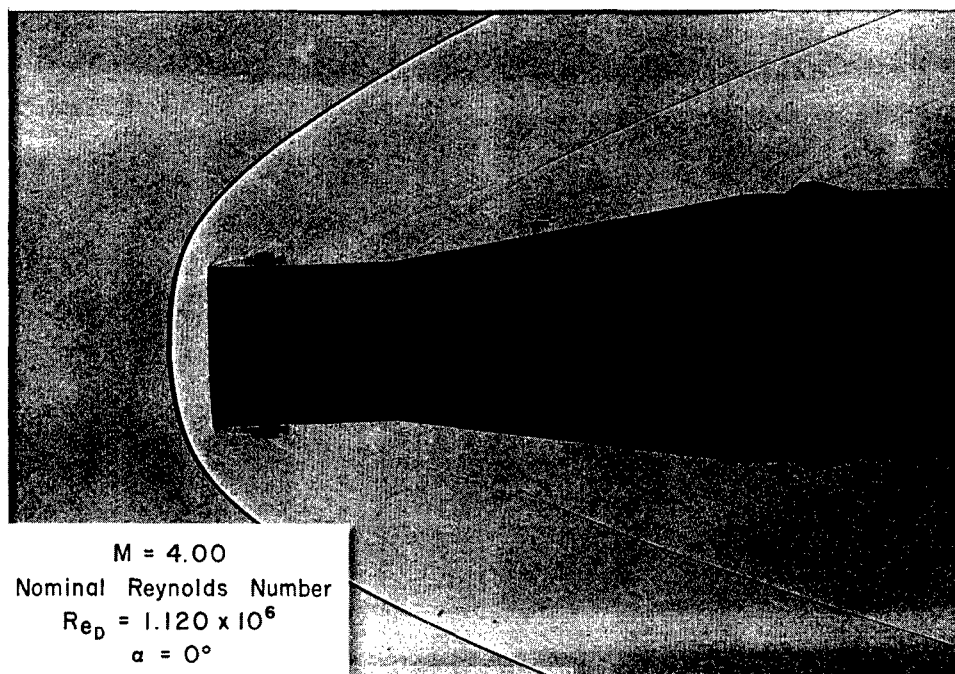
Figure 11. Selected Shadowgraphs of Launch Escape System Abort

M = 8.05
High Reynolds Number
$Re_D = 1.042 \times 10^6$
$\alpha = 0°$

M = 4.96
Nominal Reynolds Number
$Re_D = 0.882 \times 10^6$
$\alpha = 0°$

M = 4.96
Nominal Reynolds Number
$Re_D = 0.882 \times 10^6$
$\alpha = 10°$
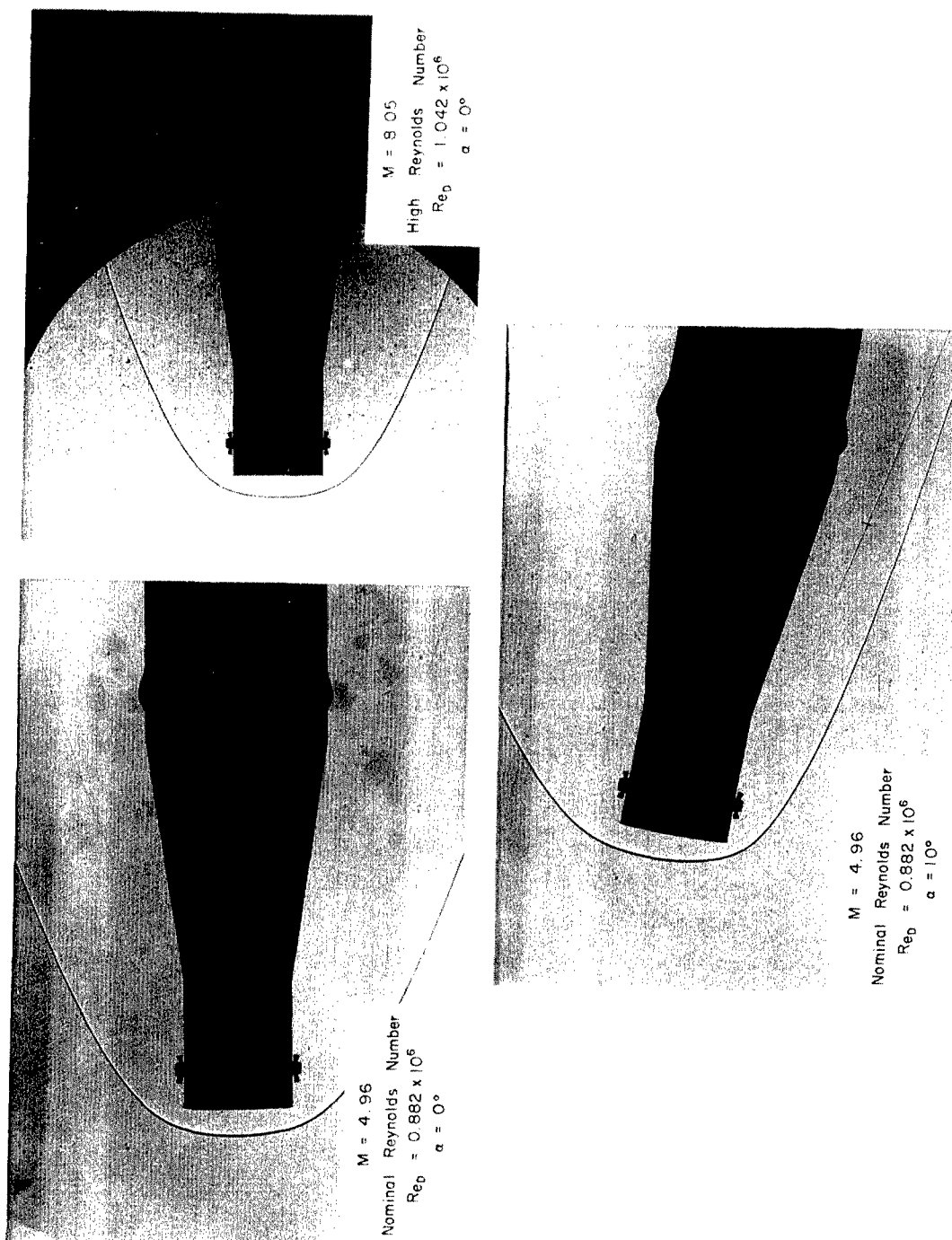
Figure 11. Launch Escape System Abort (concluded)

M = 4.00
Nominal Reynolds Number
Re_D = 1.120 x 10⁶
α = 0°

M = 4.00
Nominal Reynolds Number
Re_D = 1.120 x 10⁶
α = 10°
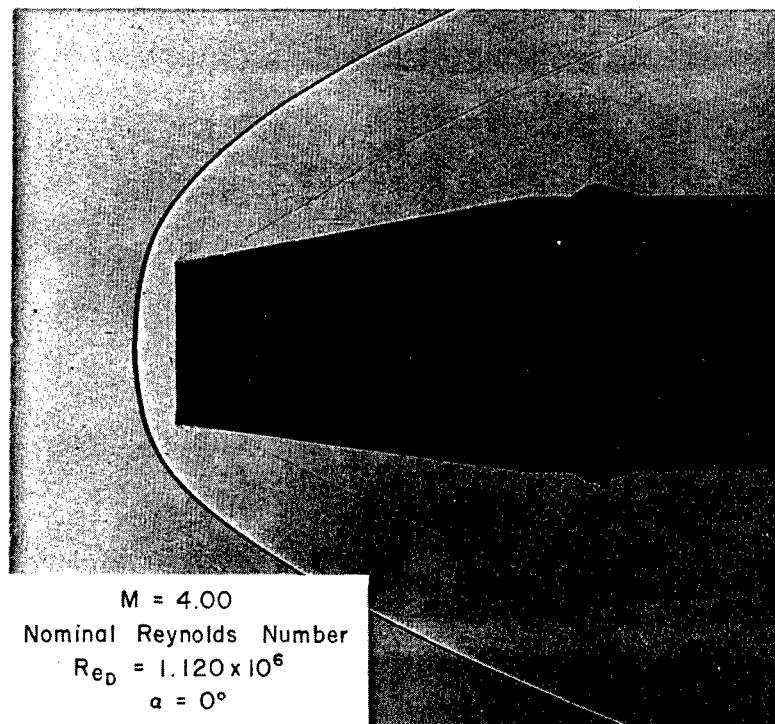
Figure 12. Selected Shadowgraphs of Service Module Abort

M = 7.08
Low Reynolds Number
$Re_D = 0.438 \times 10^6$
$\alpha = 0°$

M = 4.96
Nominal Reynolds Number
$Re_D = 0.882 \times 10^6$
$\alpha = 0°$

M = 4.96
Nominal Reynolds Number
$Re_D = 0.882 \times 10^6$
$\alpha = 10°$

Figure 12.   Service Module Abort (concluded)

APPENDIX A

DISCUSSION OF BOUNDARY LAYER SEPARATION
FROM THE LES AND REATTACHMENT ON THE CM

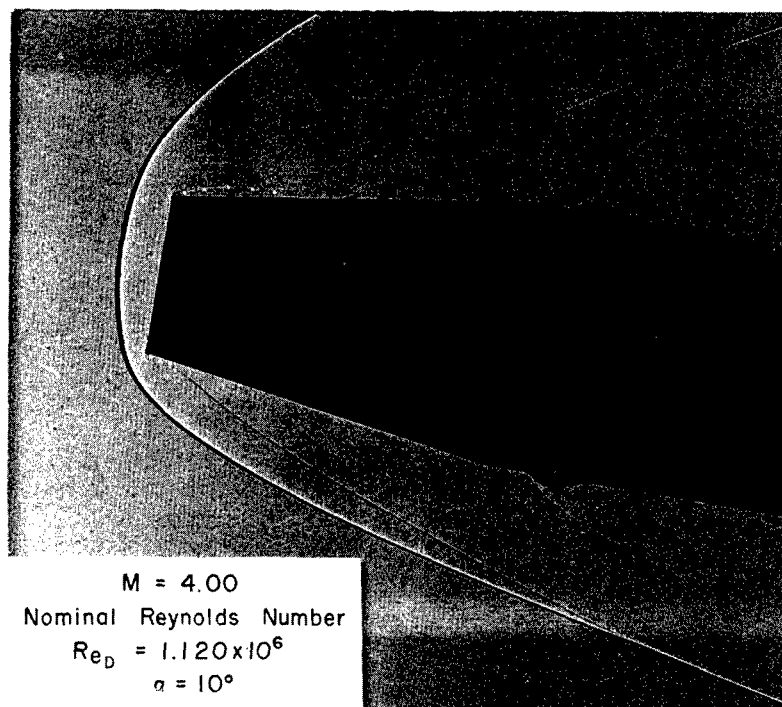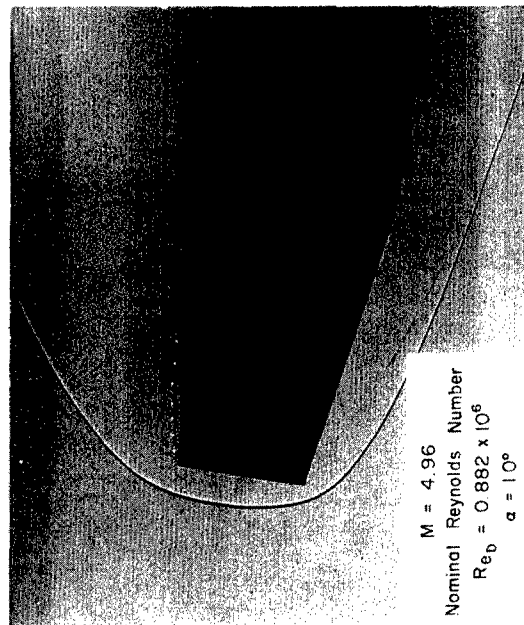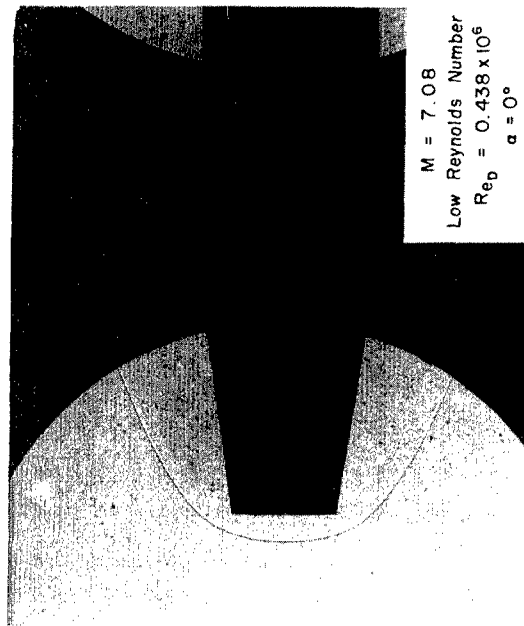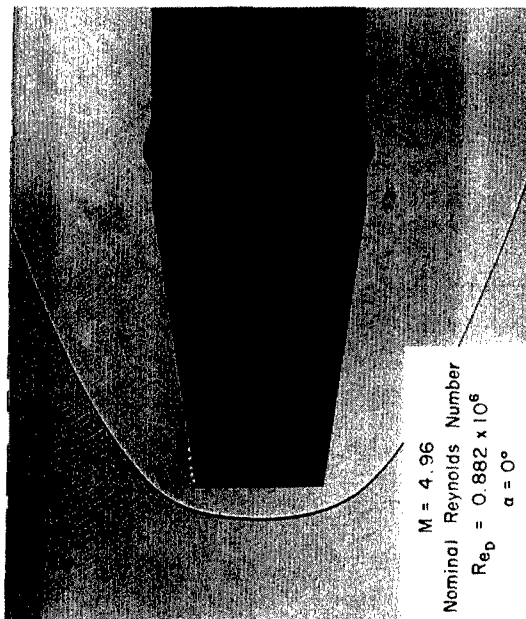The consequences of the separated flow near the nose were discussed previously. The shadowgraphs of Figure 9 were used to explain and support the characteristic "jumps" in launch configuration data. Before consideration of the factors which affect simulation of full-scale separated flows, some of the basic characteristics of separation should be reviewed as they apply to these models.

When a boundary layer is thin and attached to a surface, the static pressure distribution on that surface is given by inviscid flow theory. This fact is implicit in the normal-momentum equation of Prandtl's boundary layer theory, which states that the pressure gradient across a boundary layer is practically zero. However, in most practical cases, the static pressure distribution is either modified or determined by the interaction of the viscous layer and the external inviscid flow. The problem of separation from the LES falls into this class of viscous flows. The compression at the LES flare and the overexpansion/recompression at the cone-cylinder shoulder are the two inviscid mechanisms which provoke separation. Chemical activity, heat transfer, surface condition, radial entropy gradients, and relative boundary layer growth all modify the influence of these two mechanisms by affecting the viscous aerothermodynamic profiles.

Separation at hypersonic speeds is not a well understood phenomenon. As Cooke (Ref. 15) stated, no firm criteria have been established for either the occurence or the non-occurrence of separation. Lees and Reeves (Ref. 16) made a major advance in the theory of laminar separation in the interaction problem, but their method requires a large computer. They used an integral method and employed the Stewartson (Ref. 17) and the Cohen-Reshotko (Ref. 18) reverse-flow profiles. Correlative work, such as that of Gray (Ref. 11), gives some information about what to expect in experiments on axially symmetric bodies. Some of Gray's findings are repeated below.

At separation, the so-called dividing streamline makes a definite angle with the assumed-uniform flow upstream. This streamline separates the oncoming boundary layer from the entrained recirculating flow which diffuses across the streamline after the separation point. The streamline is located within the mixing layer, which is seen as a white trace in the shadowgraphs. The surface pressure is fairly constant in the separated zone (unless the separated volume is small) and is related to the liftoff angle of the dividing streamline for a given Mach number. In a sense, the separated layer causes the inviscid flow to "feel" a new, equivalent body.

The boundary layer thickness, which is partially controlled by density and temperature profiles, can strongly influence the extent of separation in the following manner. A blunted nose introduces negative radial entropy gradients. The corresponding positive radial total-pressure gradients approaching a frustum produce smaller initial longitudinal static pressure gradients on the frustum. The initial pressure gradient on a frustum is also a function of radial Mach number variation. A boundary layer produces such variations; hence, it follows that initial pressure gradient and separation are related to boundary layer thickness approaching the corner. Gray was able to correlate separation and corner locations in terms of their respective viscous layer thicknesses. By decreasing the flare pressures, these radial entropy gradients could conceivably lower the pressure drag on the high altitude configuration, compared with the same shape having a sharper nose. A study by Eastman and Radtke (Ref. 19) indicates such a possibility.

The detailed flow structure at reattachment is even less well known than at separation. Gray believes that reattachment is an isentropic compression. This is probably true along a streamline, but viscous layers are not isentropic across streamlines; thus, the smeared reattachment region could not be labelled "homentropic," to use the British nomenclature. By varying his flare angles, Gray found that the reattachment pressure rise had a negligible influence on the extent of separation, even though it was partially communicated upstream through the dead-air region. Extrapolating this conclusion to the present model, it can be stated that reattachment on the LES flare or the CM is a result, and not a contributing causal factor, of extent of separation.

APPENDIX B

VALIDITY OF DATA

The primary purpose of these tests was the prediction of the static aerodynamic characteristics of the full-scale Saturn IB/Apollo, a vehicle whose linear dimensions are almost 130 times those of the model. The use of a wind tunnel is a technique of partial modeling which balances economy with reliability of such predictions. Spalding (Ref. 20) defines the term "modeling" as, ". . . the practice of predicting the likely results of one experiment by way of the interpretation of the results of another experiment." The first experiment is called "full-scale" and the second is the "model" experiment. The experimenter must always ask himself whether his partial simulation of flight will give valid answers for analysis of full-scale vehicle characteristics.

It was shown in this report that large changes in stability and axial force occurred when boundary layer separation became extensive. Changes in Mach number, Reynolds number, surface conditions, and other variables, all coupled, had strong influence on the degree of separation. On the other hand, models without extensive separated flow showed only gradual changes with Mach number and negligible changes with the other variables. For flow which is fully attached to a model at moderate Mach numbers, it is immaterial whether P_∞, ρ_∞, and T_∞ are identical to the full-scale flight conditions. In the formation of aerodynamic coefficients and derivatives, pressures will be referred to their proportional free stream dynamic pressures. A good approximation to force coefficients and stability derivatives can thus be obtained by simulating geometry, Mach number, and Reynolds number, with only small perturbations contributed by non-simulation of chemistry and temperature-dependent functional relationships. Therefore, it is stated that, within random experimental error, the aerodynamic characteristics reported here for the high altitude and abort configurations are categorically valid for the full-scale case. The remaining consideration is the validity of data reported for the spike-nosed launch configuration.

A. DEGREE OF EXPERIMENTAL MODELING

Dimensional analysis, or a study of the governing differential equations, provides rules for the set-up and interpretation of experiments. Spalding's excellent discussion on modeling principles (Ref. 20) deals with combustion, but is highly applicable to high-speed aerodynamics. He reminds readers that all successful modeling of such processes has involved the deliberate violation of certain similarity rules. When boundary layers are fully attached, experimenters have been able to get away with such violation of setup rules.

This appendix centers on hypersonic flow containing a separated boundary layer. Simulation of Mach and Reynolds numbers is not always an adequate simulation for

such flow over a body less than one percent of its prototype's size. In some ranges of M and Re, it is adequate; but an important element of doubt exists for the launch configuration between Mach 4 and 6. The doubtful range can be narrowed by consideration of the character of compressible boundary layers and separated flow as described in Appendix A, and by examination of modeling principles as described by Spalding.

Physicochemical phenomena interact to produce some effect in a flow field. The importance of a given phenomenon relative to some other phenomenon can be expressed by a dimensionless group which relates quantities of mass, length, and time. A true simulation requires the maintenance of constancy of a large number of these dimensionless groups, equal to the number of applicable phenomena minus one. The experimenter can specify some groups, but is powerless to control many others.

When mass, momentum, and energy processes are coupled, a large number of rules must be obeyed for strict simulation. The phenomena which interact in full-scale vehicle flight include compressibility, viscous action, kinematics, dynamics, chemical reactions, heat transfer, conduction, and diffusion. A model in cold-flow wind tunnel cannot possibly duplicate these interactions. For example, heat transfer affects a boundary layer primarily by controlling density and viscosity variations across the layer. Chemical kinetics, conduction, diffusion, and viscous dissipation all affect heat transfer. In other words, conductivity, viscosity, and diffusivity are not independent -- they are coupled in hypersonic flow. The number of rules increases further because:

1. A dimensionless group may be important several times. Free stream thermodynamic conditions (P_∞, ρ_∞, T_∞) are not the same in the atmosphere as in the wind tunnel. If free stream Reynolds number is simulated, local body Reynolds number may not be simulated because of real gas effects in flight.

2. Unsteady processes require a time factor. This will not affect the static stability characteristics, but it will affect buffet and noise.

3. Geometric similarity is easy to control in the larger aspects, but relative roughness and its relation to boundary layer thickness is nearly impossible to control. Unscheduled transition would drastically alter separation.

4. Functional relationships need to be satisfied. For example, a viscosity-temperature relation must be the same between model and prototype. The ramifications of its non-duplication between flight and wind tunnel are raised by Hammitt (Ref. 21). Model and full-scale Reynolds numbers along a body can differ by a factor of two or three simply through the difference in viscosity variation across the shock.

The primary reason for wind tunnel testing is the provision of a cheap, quick, accurate method of prediction of full-scale vehicle characteristics. Complete modeling is impossible for a vehicle as large as Saturn. Successful partial modeling

requires recognition of the strong and weak influences. Only free stream Reynolds number and Mach number were simulated in the tests reported here. Yet, the data obtained is undoubtedly valid over most of the range of test parameters. In the uncertain range, consideration of separation characteristics and of violated modeling rules has provided enough direction to allow a reasonable choice of which data to believe.

B. ASSESSMENT OF VALIDITY OF DATA

Unfortunately, it is not easy to obtain separation or stability data from the vehicle when it is flying near Mach 5 at high altitude. It is known that a small movement in the separation locus can cause a large movement in center of pressure. Aerodynamic forces are not structurally dangerous in this flight regime, but trajectory control inputs will certainly be affected.

It was stated earlier that the data are categorically valid for the high altitude and abort configurations, and for the launch configuration below Mach 4 and above Mach 6. Local shock layer densities are considerably lower in flight than in the wind tunnel. Flight temperatures, both in the free stream and in the shock layer, are higher than in the wind tunnel. Free stream Reynolds numbers, based on vehicle diameter, were simulated in the wind tunnel around Mach 5. It is believed that local, equivalent-flat-plate Reynolds numbers along the body are smaller on the flight vehicle than on the wind tunnel model. Compared with the wind tunnel tests, the vehicle boundary layer is highly cooled in the cone-cylinder regions. Although the vehicle may be (relatively) rougher than the test model, its lower local Reynolds number implies a "stronger" laminarity in the boundary layer. Since a cooled laminar hypersonic boundary layer is somewhat more stable than an adiabatic layer, it is believed that this factor over-rides the "transition-provoking" effect of vehicle roughness.

Based on all the factors put forth in these appendixes, it is believed that maximum separation and the stability-derivative jumps will occur on the vehicle no later than at the Mach numbers where they are first predicted by the trajectory-simulating test data. The faired curves were constructed accordingly.

REFERENCES

1. Carlson, D. R. , <u>Results of a Static Longitudinal Stability and Drag Investigation of the Saturn IB Second Stage Performed in the MSFC 14-Inch Trisonic Tunnel at Mach Numbers Between 1. 93 and 4. 96.</u> MSFC Memo M-AERO-E-252-63, September 30, 1963.

2. Carlson, D. R. , <u>Hypersonic Static Longitudinal Stability and Axial Force Characteristics of Three Saturn IB Upper-Stage Models.</u> NASA TM X-53038, April 27, 1964.

3. Carlson, D. R. , <u>Supersonic Wind Tunnel Tests of Saturn IB Second Stage Configurations</u> (Basic Data Release). MSFC Memo R-AERO-AD-64-46, April 21, 1964.

4. Bills, B. C. , <u>Experimental Static Longitudinal Stability and Fore Axial Force Characteristics of the Upper Stages of the Saturn IB Vehicle in AEDC Hypersonic Tunnel E (Mach Number 5. 0 - 8. 0) </u> (Basic Data Release). MSFC Memo R-AERO-AD-64-10, February 13, 1964.

5. May, Ellery B. , and Murphree, William D. , <u>Results of Flow Calibrations in the ABMA 14 x 14 Inch Trisonic Wind Tunnel.</u> ABMA-DA-TN-65-58, September 15, 1958.

6. Anon. , <u>Arnold Center Test Facilities Handbook.</u> AEDC, USAF, January, 1961.

7. Burke, A. F. , and Bird, K. D. , <u>The Use of Conical and Contoured Nozzles in Hypervelocity Facilities.</u> CAL Report No. 112, Revised July 1962.

8. Clark, J. W. , Heaman, J. P. , and Stewart, D. L. , <u>14-Inch Wind Tunnel Spark Shadowgraph System.</u> NASA TM X-53195, January 22, 1965.

9. Mello, J. F. , <u>Investigation of Normal Force Distributions and Wake Vortex Characteristics of Bodies of Revolution at Supersonic Speeds.</u> JAS, V. 26, No. 3, March 1959.

10. Chapman, D. R. , Kuehn, D. M. , and Larson, H. K. , <u>Investigation of Separated Flows in Supersonic and Subsonic Streams with Emphasis on the Effect of Transition.</u> NACA Report 1356, 1958.

11. Gray, J. Don. , <u>A Correlation of Axisymmetric Laminar Flow Separation Characteristics.</u> AIAA Paper No. 64-475, June 29-July 2, 1964.

REFERENCES (continued)

12. Korst, H. H. , <u>A Theory for Base Pressures in Transonic and Supersonic Flow.</u> J. Appl. Mech. , V. 23, 593, 1956.

13. Fisher, L. R. , <u>Equations and Charts for Determining the Hypersonic Stability Derivatives of Combinations of Cone Frustums Computed by Newtonian Impact Theory.</u> NASA TN D-149, November 1959.

14. Hayes, W. D. , and Probstein, R. F. , <u>Hypersonic Flow Theory.</u> Academic Press, New York, 1959.

15. Cooke, J. C. , <u>Separated Supersonic Flow.</u> RAE Technical Note No. AERO 2879, March 1963.

16. Lees, Lester, and Reeves, Barry L. , <u>Supersonic Separated and Reattaching Laminar Flows: I. General Theory and Application to Adiabatic Boundary Layer-Shock Wave Interactions.</u> AIAA Preprint No. 64-4, First Annual Aerospace Sciences Meeting, New York, January 20-22, 1964.

17. Stewartson, K. , <u>Further Solutions of the Falkner-Skan Equation.</u> Proceedings of the Cambridge Philosophical Society, Vol. 50, Part 3, pp. 454-465, July 1954.

18. Cohen, C. B. , and Reshotko, E. , <u>Similar Solutions for the Compressible Laminar Boundary Layer with Heat Transfer and Pressure Gradient.</u> NACA Report 1293, 1956.

19. Eastman, D. W. , and Radtke, L. P. , <u>Effect of Nose Bluntness on the Flow Around a Typical Ballistic Shape.</u> Technical Note, AIAA J, V. 1, No. 10, October 1963.

20. Spalding, D. B. , <u>The Art of Partial Modeling.</u> Proceedings of the Ninth Symposium (International) on Combustion, Academic Press, New York, 1963.

21. Hammitt, Andrew G. , <u>Dimensionless Parameters for Viscous Similarity.</u> Technical Note, JAS, V. 27, No. 9, September 1960.